

Article

Multiple Sources of Indosinian Granites and Constraints on the Tectonic Evolution of the Paleo-Tethys Ocean in East Kunlun Orogen

Guochao Chen ^{1,2,3,*}, Xianzhi Pei ^{1,*}, Ruibao Li ¹, Zuochen Li ¹, Youxin Chen ¹ , Chengjun Liu ¹ and Lei Pei ¹

¹ Key Laboratory of Western Mineral Resources and Geological Engineering, Ministry of Education, School of Earth Science and Resources, Chang'an University, Xi'an 710054, China

² School of Civil Engineering, Nanyang Institute of Technology, Nanyang 473000, China

³ Key Laboratory of Metallogeny and Mineral Assessment, Ministry of Natural Resources, Beijing 100037, China

* Correspondence: chaoschen@126.com (G.C.); peixzh@sina.com (X.P.)

Abstract: Numerous Indosinian granitoids occur in the East Kunlun Orogen (EKO). The Indosinian was a key transitional period associated with the evolution of the Paleo-Tethys Ocean. Here, we study the relationship between the petrogenesis of the granitoids and the regional tectonic setting based on a comprehensive analysis of the petrology, geochronology, and geochemistry of typical granitoids in the eastern part of the EKO. The Indosinian granitoid compositions are dominated by quartz diorites, granodiorites, monzogranites, porphyritic monzogranites, and syenogranites. Early Indosinian granitoids are large, granitic batholiths, while the middle and late Indosinian granitoids are smaller in size. From the early Indosinian to late Indosinian, the granitoids show a transition from a medium-K calc-alkaline to high-K calc-alkaline composition. They are enriched in light rare earth elements (LREEs) and large-ion lithophile elements (LILEs) and depleted in high-field-strength elements (HFSEs), especially for the Helegangxilikete and the Kekeelalong plutons. The late Indosinian granitoids have relatively low Y and Yb contents, high Sr contents, and high La/Yb and Sr/Y ratios, which suggests adakitic affinity. The zircon saturation temperatures of the early Indosinian syenogranite and the Keri syenogranite are above 800 °C. The zircon saturation temperatures of other Indosinian granites (average 749 °C) are lower than those of the biotite and amphibole partial melting experiment. In the early Indosinian (255–240 Ma), numerous granitoids were the products of the partial melting of the juvenile lower crust by mafic magma underplating. This underplating is geodynamically related to the continuous subduction of a branch of Paleo-Tethys Ocean, with slab break-off, rapid upwelling, and mantle decompression. In the middle Indosinian (240–230 Ma), the compression that accompanied the continent–continent collision was not conducive to fluid activity, and hence, the formation of magma could be attributed to dehydration partial melting of muscovite, biotite, or amphibole. In the late Indosinian (230–200 Ma), the delamination of thickened crust would provide heat and channels for fluid migration, leading to a flare-up of the magmas. The composition and petrogenesis of the Indosinian granitoids in the eastern EKO are the result of processes associated with the subduction, collisional, and post-collisional stages, during the evolution of the Paleo-Tethys Ocean.



Citation: Chen, G.; Pei, X.; Li, R.; Li, Z.; Chen, Y.; Liu, C.; Pei, L. Multiple Sources of Indosinian Granites and Constraints on the Tectonic Evolution of the Paleo-Tethys Ocean in East Kunlun Orogen. *Minerals* **2022**, *12*, 1604. <https://doi.org/10.3390/min12121604>

Academic Editor: Jaroslav Dostál

Received: 8 October 2022

Accepted: 8 December 2022

Published: 14 December 2022

Publisher's Note: MDPI stays neutral with regard to jurisdictional claims in published maps and institutional affiliations.



Copyright: © 2022 by the authors. Licensee MDPI, Basel, Switzerland. This article is an open access article distributed under the terms and conditions of the Creative Commons Attribution (CC BY) license (<https://creativecommons.org/licenses/by/4.0/>).

Keywords: East Kunlun Orogen (EKO); Indosinian; granitoids; adakite; petrogenesis; geochemistry; tectonic evolution

1. Introduction

Granites provide insight into the formation of the continental crust. The petrology and geochemistry of these rocks record the origin and evolution of the associated magma [1–5]. The formation of granitoids is a complex process related to the source composition, melting temperature, pressure in the source area, and water availability [6–8]. Previous research has

demonstrated that the formation of granitoids corresponds to particular tectonic settings, with different types of granites associated with different tectonic environments. Historically, it was widely accepted that I-type granites formed in subduction-related settings and S-type granites in collisional settings. Geologists believe that the I-type and S-type granites formed in compressional tectonic environments. In contrast, the evolution of A-type granites is thought to be unrelated to orogenic activity and occurred in response to hotspot activity, rifting, or other tensional tectonic settings. However, some studies have indicated that no genetic relationship exists between the formation of granitoids and their tectonic environments [9,10]. Thus, there are some limitations in using single granites to determine tectonic environments [11]. However, granitoid composition can be affected by many factors, including tectonic setting, the composition of the source material, and water availability. For example, granite would have a high-K calc-alkaline composition due to the increasing maturity of the crust in the post-collisional stage. The direction of magma migration is consistent with that of plate subduction and opposite that of slab retreat. Slab break-off can give rise to a large volume of magma in short periods [12].

The East Kunlun Orogen (EKO) is rich in magmatic rocks and is a natural laboratory for the study of tectonic evolution. These studies would also contribute to a great understanding of how the Paleo-Tethys Ocean evolved in the Late Paleozoic. Thus, we systematically studied the spatial and temporal distribution of the granitoids, their magmatic sources, and petrogenesis of these granites in order to determine the Indosinian tectonic settings in the EKO.

2. Geological Setting and Field Characteristics

The EKO is located on the northeast margin of the Tibetan Plateau. It is an integral part of the Central China Orogenic Belt, lying between the Qaidam block to the north and the Bayan Har block to the south. To the west, it connects the West Kunlun Orogenic with the Altyn strike-slip fault. The eastern part of the EKO adjoins the Gonghe Basin and Wenquan fault. The EKO has an East–West-trending orientation and a length of more than 1200 km. Three major tectonic boundaries have been identified in the EKO. From north to south, they are the northern East Kunlun fault zone (NEKF), the central East Kunlun fault zone (CEKF), and the southern East Kunlun fault zone (SEKF) (Figure 1). The three fault zones can be used to divide the EKO into four sub-tectonic units from north to south: North Kunlun belt (NKB), Central Kunlun belt (CKB), South Kunlun belt (SKB), and Buqingshan tectonic mélange belt (BTM) (Figure 1b) [13–18].

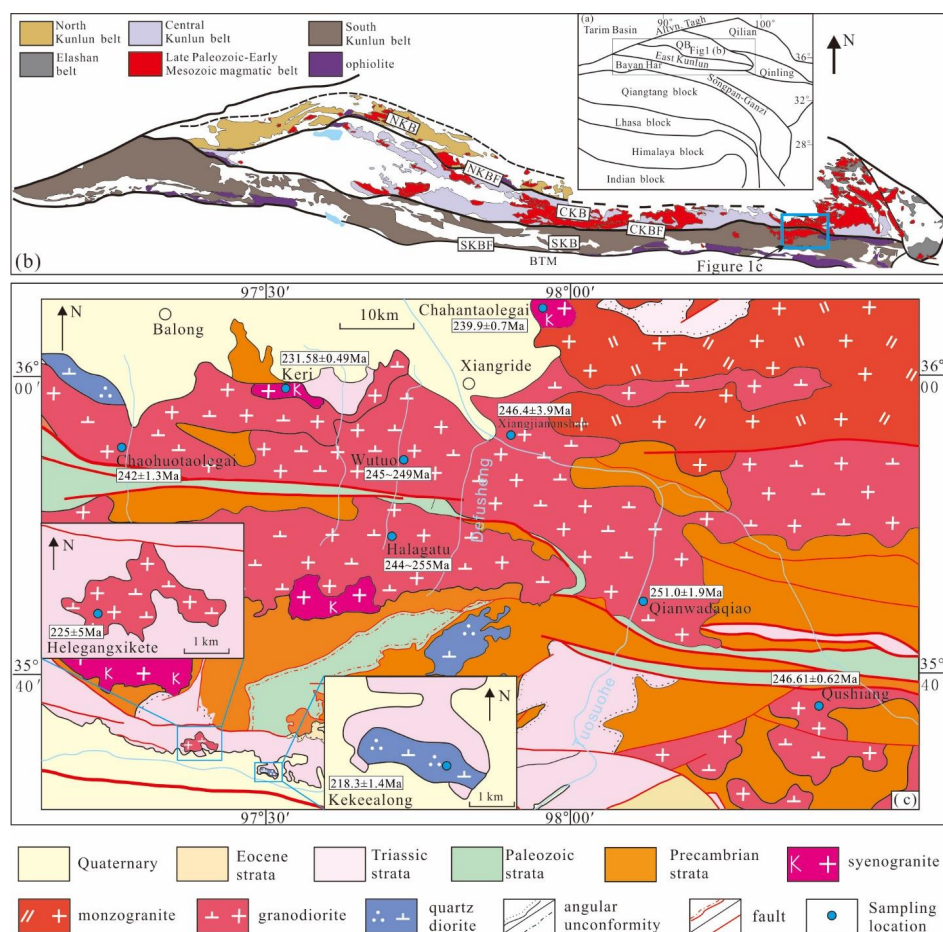


Figure 1. (a) Tectonic location of the East Kunlun Orogen in China; (b) Distribution of granites of late Paleozoic to early Mesozoic in the Eastern Kunlun; (c) Simplified geological map for the eastern part of the EKO (modified from Li et al. [19]). Data sources for the zircon U-Pb ages are as follows: Halagatu pluton (after [19]); Xiangjiananshan pluton (after [20]); Wutuo pluton (after [20,21]); Qushiang pluton (after [22]); Chaohuotaogai pluton (after [23]); Chahantaolegai pluton (after [24]); Keri pluton (after [25]); Kekealong pluton (after [26]); Helegangxikete pluton (after [27,28]).

The EKO experienced two tectonic stages during the Paleozoic to Early Mesozoic, which resulted in the development of the Proto-Tethys and the Paleo-Tethys. The magmatic processes and sedimentary sequences that accompanied the development of these two events are complex. The CEKF is an early Paleozoic suture zone that may be related to the northward subduction of the Proto-Tethys Ocean. Back-arc extension accompanying the subduction further resulted in the formation of a small ocean basin [29–32]. As a result of a prolonged period of evolution, the BTM preserves geological evidence of the Proto- and Paleo-Tethys oceans [33–36].

The EKO ophiolites with an age of 522–509 Ma indicate that the Proto-Tethys Ocean opened before the Middle Cambrian. From 487 Ma to 430 Ma, a set of arc magmatic rocks was formed in the EKO, indicating that the subduction of the Proto-Tethys Ocean started at least in the Early Ordovician and continued until the Middle Silurian [22]. During 430–390 Ma, magmatic activity changed obviously, and A-type granite and adakite magmatic rocks appeared. In addition, sedimentary records show that the Devonian Maoniushan Formation is a molasse sequence, indicating that the EKO entered the post-collision stage of Proto-Tethys [18].

During the Late Paleozoic to Mesozoic, the EKO was in the stage of the Paleo-Tethys Ocean. According to the chronological records of ophiolites in the EKO, the Paleo-Tethys Ocean in EKO began opening before the Carboniferous. Due to the northward subduction

of the Paleo-Tethys Ocean, the EKO formed a set of arc magmatic rocks with ages ranging from 270 to 240 Ma, and the magmatic mixing of these magmatic rocks was significant. With the collision between the Bayan Har/Qiangtang and East Kunlun blocks, the Paleo-Tethys Ocean began to close, and the EKO entered the stage of intracontinental evolution, forming A-type granite and adakitic magmatic rocks with post-collision characteristics [19,20].

The basement of the EKO is composed of Paleoproterozoic–Neoproterozoic metamorphic rocks. The most widespread of these rocks are the Paleoproterozoic Baishahe Formation (Pt_1b), the Mesoproterozoic Xiaomiao Formation (Pt_2x) of the Changcheng System, the Mesoproterozoic Langyashan Formation (Pt_2l) of the Jixian System, the Mesoproterozoic Kuhai Group (Pt_2K), the Neoproterozoic Wanbaogou Group (Pt_3W), and the Quidonggou Formation (Pt_3qj). The lower Paleozoic Nachitai Group (Pz_1N) volcanic sedimentary rock, Maoniushan Formation (Dm) continental clastic rock, and intermediate acid volcanic rock are related to the development of the Paleo-Tethys. The early geological history of the Paleo-Tethys Ocean is recorded in the sedimentary rocks of the Carboniferous Haerguole Formation (C_1hl) and Haoteluowa Formation (C_2ht), the middle and lower Permian Maerzheng Formation ($P_{1-2}m$) turbidite, and the upper Permian Gequ Formation (P_3g). The later evolution of the Paleo-Tethys Ocean is recorded in the lower Triassic Hongshuichuan Formation (T_1h), the middle Triassic Naocangjiangou Formation (T_2n), the middle Triassic Xilikete Formation (T_2x), the upper Triassic Babaoshan Formation (T_3b), the upper Triassic Elashan Formation (T_3e), and the lower Jurassic Yangqu Formation (J_1y). In addition, there are several angular unconformities between the Gequ Formation and Haoteluowa Formation, the Xilikert Formation and Naocangjiangou Formation, and the Babaoshan Formation and underlying strata, and parallel unconformities between the Yangqu Formation and Babaoshan Formation in the EKO.

Magmatic activity was frequent in the EKO. The granitoids dominate the EKO with few mafic and ultramafic rocks. Due to the multi-stage tectonic activity of the EKO, the magmatic activity spans an extensive time period. Magmatic activity occurred from the Jinning period to the Yanshanian period [18,22], with the most intense magmatic activity occurring in the Indosinian. The igneous rocks with different ages have different characteristics:

(1) The Precambrian granitoids are gneissic, due to the effects of multi-stage tectonic events; (2) the early Paleozoic magmatic rocks in the EKO include ultramafic and mafic lithologies, diorite, granite, and monzonite; (3) granodiorites are the most common magmatic rocks during the late Paleozoic-early Mesozoic.

We combined our research with nine granites and 107 rock geochemical samples (Supplementary Table S1) obtained from the eastern EKO to understand the petrogenesis of the Indosinian granites. Samples in this study were taken from fresh outcrops without visible alteration. Fresh whole-rock samples were powdered to less than 200-mesh size for whole-rock chemical analyses. The analytical precision and accuracy for major elements were generally better than 5%, and those for most trace elements were better than 2%. The rocks in the CEKB and SEKB were formed during the Indosinian. The early Indosinian granites (255–240 Ma) are generally large batholiths, some of which have complex lithologies, such as the Wutuo (245–251 Ma), Xiangjiananshan (246.4 ± 3.9 Ma), and Halagatu (244–255 Ma) plutons. In contrast, the Chaohuolutaogai (242 ± 1.3 Ma) and Qushiang (246.61 ± 0.62 Ma) plutons are relatively small in size. The early Indosinian plutons intrude into the basement rocks of the EKO. The plutons that developed in the middle (240–230 Ma, Chahantaolegai (239.9 ± 0.7 Ma) and Keri (231.58 ± 0.49 Ma) plutons) and late Indosinian (230–201 Ma, Helegangxikete (225 ± 5 Ma) and Kekeelong (218.3 ± 1.4 Ma) plutons) are small in size and exposed as small plutons or stocks. The formation age of these granitoids ranged from 255 to 218 Ma (Table 1). Wall rocks of these plutons are basement rock, early Triassic intrusive rock, and Triassic sedimentary strata (Figure 1c).

Mafic magmas are also exposed in the eastern part of the EKO. Compared to the granite, mafic rock exposures are limited in extent and occur as small plutons and veins [37,38].

Table 1. Geological characteristics of the Indosinian granite in eastern region of EKO [19–28].

| Locality | Rock | Texture | Structure | MMEs | Host rock | Method | Age (Ma) | Tectonic Unit | Reference |
|------------------|--------------------------|------------------|-------------|-----------|--|-----------|----------------------------|---------------|-----------|
| Halagatu | granodiorite | medium | massive | inclusion | basement | LA-ICP-MS | 247.2 ± 1.5 255.6 ± 1.9 | SKB | [19] |
| | porphyritic monzogranite | medium to coarse | porphyritic | inclusion | granodiorite | LA-ICP-MS | 244.3 ± 2.2 | | |
| | monzogranite | coarse | massive | inclusion | granodiorite | | | | |
| | syenogranite | medium to coarse | massive | no | granodiorite | | | | |
| Wutuo | granodiorite | medium to fine | massive | inclusion | basement | LA-ICP-MS | 249 ± 1 | CKB | [21] |
| | porphyritic monzogranite | medium to coarse | porphyritic | inclusion | granodiorite | LA-ICP-MS | 247 ± 1 | | |
| | syenogranite | medium to coarse | massive | inclusion | granodiorite | LA-ICP-MS | 245 ± 1 | | |
| Xiangjiananshan | granodiorite | medium to coarse | massive | inclusion | basement | LA-ICP-MS | 251 ± 1.9 | CKB | [20] |
| | porphyritic monzogranite | medium to coarse | massive | inclusion | granodiorite | | | | |
| | monzogranite | medium to coarse | massive | inclusion | granodiorite | LA-ICP-MS | 246.4 ± 3.9 | | [20] |
| | syenogranite | coarse | massive | inclusion | granodiorite | | | | |
| Qushiang | granodiorite | medium to coarse | gneissic | inclusion | basement | LA-ICP-MS | 246.61 ± 0.62 | CKB | [22] |
| Chaohuolutaogai | granodiorite | medium to coarse | massive | inclusion | basement and Early Triassic magmatic rocks | LA-ICP-MS | 241.2 ± 0.8 | CKB | [23] |
| Chahantaolegai | syenogranite | medium to coarse | massive | no | basement and Early Triassic magmatic rocks | LA-ICP-MS | 239.9 ± 0.7 | CKB | [24] |
| Keri | syenogranite | medium to coarse | massive | inclusion | basement | LA-ICP-MS | 231.58 ± 0.49 | CKB | [25] |
| Helegangxilikete | granodiorite | medium to fine | massive | inclusion | Middle Triassic Naocangjiangou Formation | LA-ICP-MS | 225 ± 2 | SKB | [27,28] |
| Kekeearlong | quartz diorite | medium to fine | massive | no | Middle Triassic Naocangjiangou Formation | LA-ICP-MS | 218.3 ± 1.4 | SKB | [26] |

MMEs—mafic microgranular enclaves

3. Petrography

Most of the granitoids in the eastern part of the EKO are characterized by medium-to coarse-grained texture and massive structure (Figure 2). The Halagatu, Wutuo, and Xiangjiananshan plutons are complex granites, with the most common rock types being granodiorite, monzogranite, porphyry monzogranite, and syenogranite (Table 1). The Chahantaolegai and Keri plutons are both syenogranites; the Helegangxilikete, Chaohuolutaogai, and Qushiang plutons are granodiorites; the Kekeearlong pluton is a quartz diorite. The main mineral composition of the plutons is similar, including plagioclase, K-feldspar, quartz, hornblende, and biotite. The content of plagioclase and hornblende is relatively high in the mafic rocks, with feldspar and quartz increasing as the rock types become more acidic in composition (Table 1). Most of the plutons, excluding the Chahantaolegai and Kekeearlong, contain mafic microgranular enclaves (MMEs).



Figure 2. Outcrop photos for the Indosinian granite in the eastern region of the EKO. (a) Xiangjiananshan granodiorite; (b) Xiangjiananshan monzogranite; (c) Wutuo granodiorite; (d) Wutuo monzogranite; (e) Wutuo syenogranite; (f) Qushiang gneissic granodiorite; (g) Chaohuolutaogai granodiorite; (h) Chahantaolegai syenogranite; (i) Keri syenogranite.

4. Whole-Rock Geochemistry

4.1. Major Elements

The results for the major elements in the felsic rock have a negative correlation between SiO_2 and oxides. The SiO_2 content of early Indosinian plutons is in the range of 60.26–76.27 wt.%. The values of the A/CNK ratios range from 0.91–1.08, with an average of 0.99. The values for $\text{Mg}^{\#}$ ($\text{Mg}^{\#} = \text{atomic } 100 \times \text{Mg}^{2+}/(\text{Mg}^{2+} + \text{TFe}^{2+})$) range from 4–44 with an average of 32. The $\text{Mg}^{\#}$ values of the Qushiang pluton are high, with an average value of 43. In the A/NK-A/CNK diagram (Figure 3a), the granodiorite is classified as met-

aluminous calc to calc-alkaline series, while the monzogranite, porphyritic monzogranite, and syenogranite are classified as weakly peraluminous alkaline-calc to calc-alkaline series (Figure 3b,c). In the TAS diagram (Figure 3d), they plot as diorite, granodiorite, and granite. The MgO , CaO , P_2O_5 , TiO_2 , Al_2O_3 , and FeO^T contents in the different rocks decrease as the SiO_2 content increases, while the Na_2O content increases as the SiO_2 content increases (Figure 4), which indicates that fractional crystallization of plagioclase, biotite, and apatite may have occurred.

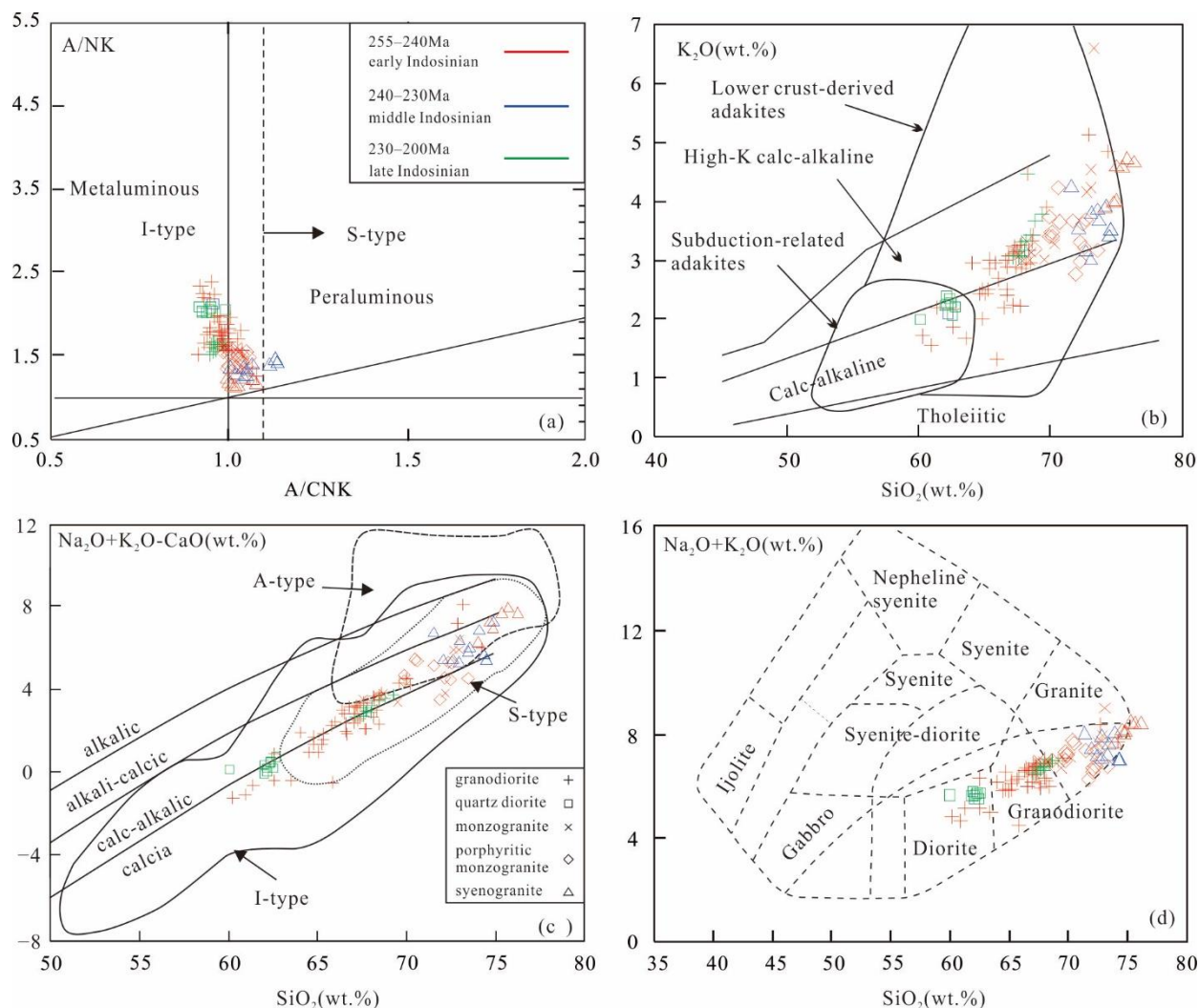


Figure 3. Diagrams of A/NK vs. A/CNK. $A/\text{CNK} = \text{Al}_2\text{O}_3/(\text{CaO} + \text{Na}_2\text{O} + \text{K}_2\text{O})\%$ in molar; $A/\text{NK} = \text{Al}_2\text{O}_3/(\text{Na}_2\text{O} + \text{K}_2\text{O})\%$ in molar. (a) (after [39]) K_2O vs. SiO_2 ; (b) (after [40]) ($\text{Na}_2\text{O} + \text{K}_2\text{O} - \text{CaO}$) vs. SiO_2 ; (c) (after [41]) ALK vs. SiO_2 ; (d) (after [42]) for the Indosinian granite in the eastern region of the EKO.

In contrast, the middle Indosinian granite is dominated by granite in rock type, with the major element concentrations showing a small variation range. The contents of SiO_2 (71.52–74.90 wt.%), K_2O (2.99–4.58 wt.%), and Na_2O (3.31–4.14 wt.%) are high, while the content of Al_2O_3 (12.87–3.88 wt.%), FeO^T (1.65–2.74 wt.%), MgO (0.09–0.68 wt.%), and CaO (0.76–1.93 wt.%) are low. The values of the A/CNK are relatively high (1.00–1.13). The $\text{Mg}^\#$ values are lower (9–34), with an average of 21. In the A/NK-A/CNK diagram, the Keri pluton is classified as mildly peraluminous granite, while others are classified as strongly peraluminous granite. All samples are assigned to the high-K calc-alkaline series. In the TAS diagram, the samples are plotted in the granite field (Figure 3d).

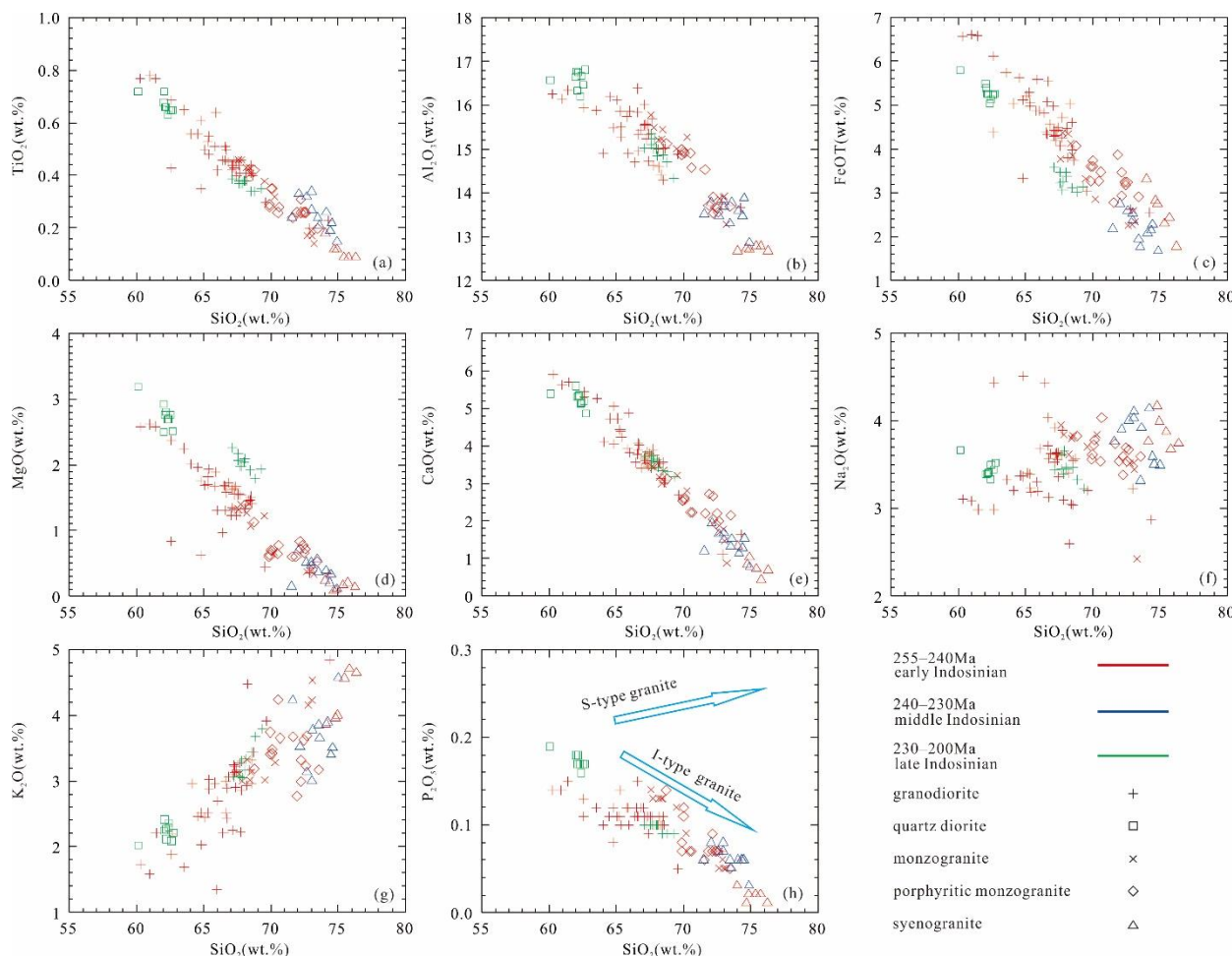


Figure 4. Harker diagrams for the Indosinian granite in the eastern region of the EKO. (a) SiO_2 vs. TiO_2 diagram; (b) SiO_2 vs. Al_2O_3 diagram; (c) SiO_2 vs. FeOT diagram; (d) SiO_2 vs. MgO diagram; (e) SiO_2 vs. CaO diagram; (f) SiO_2 vs. Na_2O diagram; (g) SiO_2 vs. K_2O diagram; (h) SiO_2 vs. P_2O_5 diagram.

The SiO_2 (60.08–69.28 wt.%), K_2O (2.00–3.79 wt.%), and Na_2O (3.22–3.66 wt.%) content of late Indosinian rocks is moderate, while the content of Al_2O_3 (14.33–16.81 wt.%), MgO (1.78–3.20 wt.%), and CaO (3.17–5.61 wt.%) is high. The values of the A/CNK are relatively low (mostly <1.0), consistent with a metaluminous granite composition. The $\text{Mg}^{\#}$ values range from 45 to 55. The composition of the Helegangxilikete pluton is high-K calc-alkaline, while the Kekeearlong pluton plots close to the boundary between middle- and high-K calc-alkaline. In the TAS diagram, they plot in the diorite and granodiorite areas, respectively (Figure 4c).

4.2. Trace Elements

The total REE content of the early Indosinian granitoids ranges from 70.57 to 274.41 ppm, with an average value of 122.01 ppm. The $(\text{La}/\text{Yb})_{\text{N}}$ ratio varies greatly, averaging 10.39. The chondrite-normalized REE distribution diagram indicates that the early Indosinian granitoids are enriched in light rare earth elements (LREEs) (Figure 5a), but depleted in heavy rare earth elements (HREEs). Granodiorite has a slight negative Eu anomaly, but syenogranite has an obvious negative Eu anomaly. Except for the Wutuo monzogranite, which had a lower δEu value, other monzogranite has a higher δEu value than granodiorite, which has an insignificant negative or positive Eu anomaly.

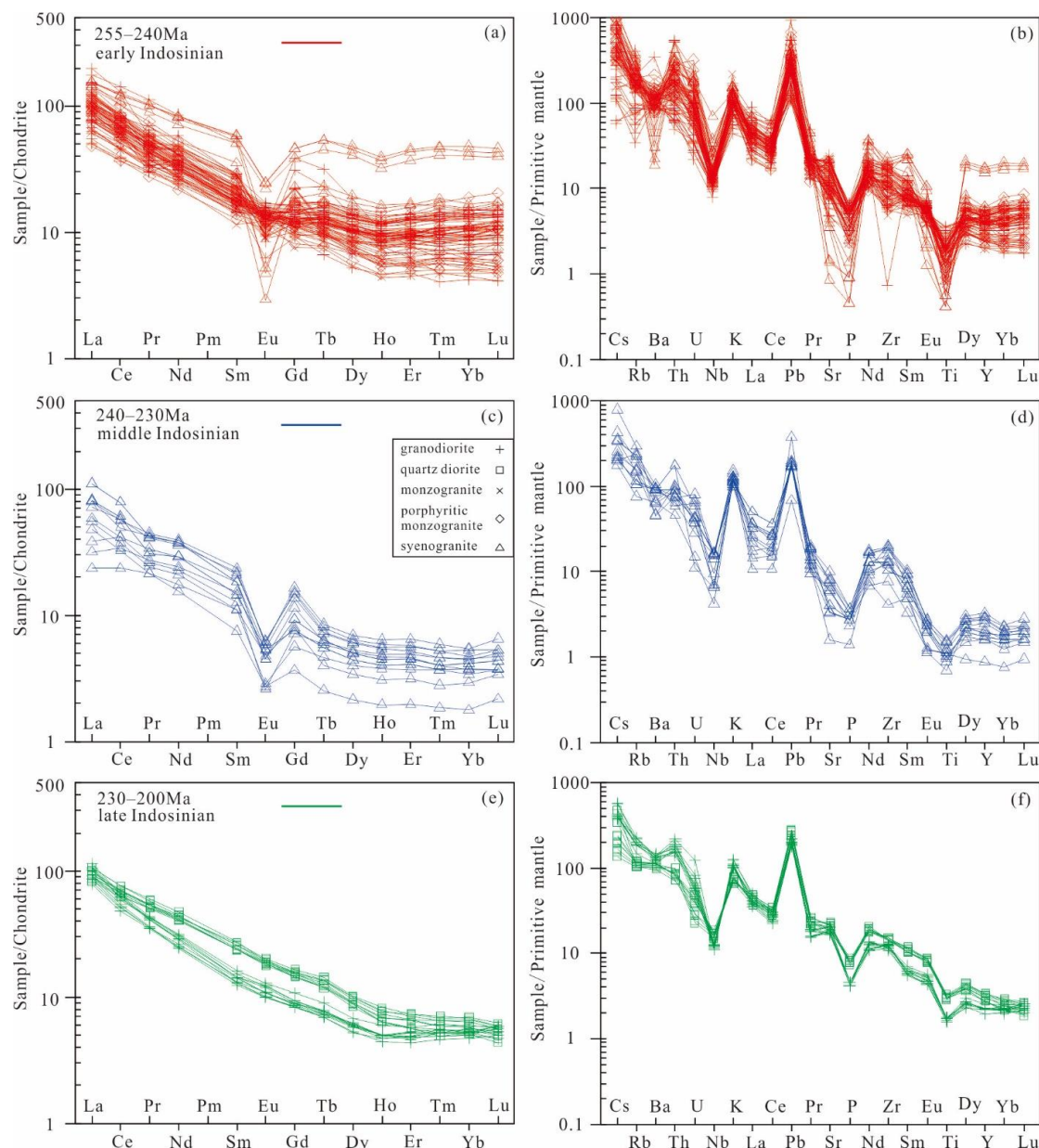


Figure 5. Chondrite-normalized REE distribution patterns ((a,c,e), normalization values after [43]); primitive mantle-normalized trace element spider diagrams ((b,d,f), normalization values after [44]) for the Indosinian granite in the eastern region of the EKO.

In the primitive mantle-normalized trace element distribution diagram (Figure 5b), the granitoids are enriched in large-ion lithophile elements (LILEs), but depleted in high-field-strength elements (HFSEs) (i.e., Nb, Ta, and Ti). These anomalies may be related to the metasomatism of subducted fluids [7]. In addition, the Rb content ranges from 21.88–263.00 ppm, the Sr content ranges from 18.20–518.11 ppm, the Y content ranges from 3.95–80.6 ppm, the Rb/Sr ratio ranges from 0.06–10.88, and the Sr/Y ratio ranges from 0.85–50.33.

The chondrite-normalized REE patterns of the middle Indosinian granitoids are similar to those of the early Indosinian granitoids (Figure 5c,d), but the total REE content is slightly lower than that of the early Indosinian granitoids, ranging from 41.84 to 129.80 ppm, with an average of 86.34 ppm. The ratio of $(\text{La}/\text{Yb})_{\text{N}}$ ranges from 7.20–27.11, with an average of 17.26. The Sr and Y content of middle Indosinian granitoids is low, namely 33.61–210.79 ppm and 3.95–14.83 ppm, respectively. The Rb content for these granitoids

ranges from 47.93–185.10 ppm, the Rb/Sr ratio ranges from 0.35–5.51, and the Sr/Y ratio ranges from 3.58–32.10.

The total REE content of late Indosinian granitoids ranges from 93.15–148.89 ppm, with an average of 121.31 ppm. The $(\text{La}/\text{Yb})_{\text{N}}$ ratio of these granitoids is high, ranging from 11.86 to 24.28, with an average of 17.14, indicating that fractionation crystallization occurred between the heavy and light rare earth elements. The trace element compositions of the late Indosinian granitoids are similar to those of the early Indosinian granitoids (Figure 5f). The granitoids have a high Sr content (348–485 ppm, average 411 ppm), a high Sr/Y ratio (27.30–43.40, average 35.17), and a low Y content (8.94–15.60 ppm, average 11.94 ppm).

5. Magma Source and Petrogenesis

5.1. Granite Type

There are no peraluminous minerals (such as garnet and cordierite) in the Indosinian granitoids of the eastern EKO. Most of these rocks contain amphibole, and the P_2O_5 content of the plutons is relatively low, with a negative correlation between SiO_2 and P_2O_5 (Figure 4h). The A/CNK value of the granitoids is less than 1.1, with an average of 0.95, except for the Chahantaolegai pluton (1.05–1.13, average 1.1). These values are consistent with an I-type granite composition rather than an S-type composition (Figure 3a) [4]. However, the early Indosinian plutons, except for the syenogranite, have $\text{FeO}^{\text{T}}/\text{MgO}$ (average 4.06) and $10,000 \times \text{Ga}/\text{Al}$ ratios (average 2.10) are close to the I-type granite (2.27 and 2.18, respectively) [45]. The compositions of the rocks mainly fall in the I-type and S-type granite regions in Figure 6. Moreover, the average zircon saturation temperature of the whole rock was 753 °C, lower than the average formation temperature of A-type granites (i.e., 800 °C [46]) but similar to that for I-type granite (764 °C [47]). The early Indosinian syenogranite (Halagatu and Wutuo plutons) has high $\text{FeO}^{\text{T}}/\text{MgO}$ ratios (average 23.09) and $10,000 \times \text{Ga}/\text{Al}$ ratios (average 2.87). The zircon saturation temperature of the whole rock was higher than 800 °C, similar to that of A-type granites (Figure 6). Regional data show that the A-type granites were exposed not only during the early Indosinian, but also during the late Indosinian [48]. The middle Indosinian Chahantaolegai syenogranite has high SiO_2 content and A/CNK ratios (average ratio 1.10), similar to values for S-type granites (Figure 3a). Regional data for the eastern part of the EKO show that the early Indosinian granitoids are mainly I-type granites with a small number of A-type granites, that the middle Indosinian granitoids are mainly I-type and S-type granites, and that the late Indosinian granitoids are mainly I-type granites with minor A-type granites also present.

5.2. Magma Source

The Indosinian granitoids in the eastern EKO have a high SiO_2 content with enrichment in Th, U, K, and Pb and depletion in Nb, Ta, and Ti. These characteristics resemble the composition of crust-derived magmatic rocks (Figure 5) [49]. The granodiorite has a composition consistent with an I-type granite and, hence, may be derived from the partial melting of meta-igneous rocks [46,50]. These granodiorites have low $\text{K}_2\text{O}/\text{Na}_2\text{O}$ ratios, similar to the composition of melts derived from metabasalts yet different from that derived from pelites [51]. In the plots of $(\text{Na}_2\text{O} + \text{K}_2\text{O})/(\text{FeO} + \text{MgO} + \text{TiO}_2)$ vs. $\text{Na}_2\text{O} + \text{K}_2\text{O} + \text{FeO} + \text{MgO} + \text{TiO}_2$ and $\text{Al}_2\text{O}_3/(\text{FeO} + \text{MgO} + \text{TiO}_2)$ vs. $\text{Al}_2\text{O}_3 + \text{FeO}^{\text{T}} + \text{MgO} + \text{TiO}_2$ (Figure 7a,b), the granodiorite has a composition consistent with the partial melting of mafic components. The granodiorites have low molar $\text{Al}_2\text{O}_3/(\text{MgO} + \text{FeO}^{\text{T}})$ ratios, high molar $\text{CaO}/(\text{MgO} + \text{FeO}^{\text{T}})$ ratios (Figure 7c), high $\text{CaO}/\text{Na}_2\text{O}$ ratios, and low $\text{Al}_2\text{O}_3/\text{TiO}_2$ ratios (Figure 7d), compositions similar to magmas derived from metabasalts [52]. These data indicate that the main source for the granodiorite was likely mafic rock. The investigation demonstrated that the amount of $\varepsilon_{\text{Hf}}(t)$ and $\varepsilon_{\text{Nd}}(t)$ in the late Paleozoic-early Mesozoic granites of the EKO are relatively low (i.e., $\varepsilon_{\text{Hf}}(t) = -3.2$ to 0; $\varepsilon_{\text{Nd}}(t) = -5.3$ to -2.1 [20,53]). The data are similar to those obtained for mafic magmatic rocks in the same period of the EKO (i.e., $\varepsilon_{\text{Hf}}(t) = -4.4$ to 1.1; $\varepsilon_{\text{Nd}}(t) = -7.4$ to 2.9 [20]), but significantly different from those

of the mid-oceanic ridge basalts (MORB) [54]) and the EKO basement rocks (i.e., basement $\varepsilon_{\text{Hf}}(t) = -15.51$; mid-oceanic ridge basalts $\varepsilon_{\text{Nd}}(t) = 12.2$ to 12.8 [55,56]). Therefore, the source area for the granodiorite may have been juvenile mafic lower crust.

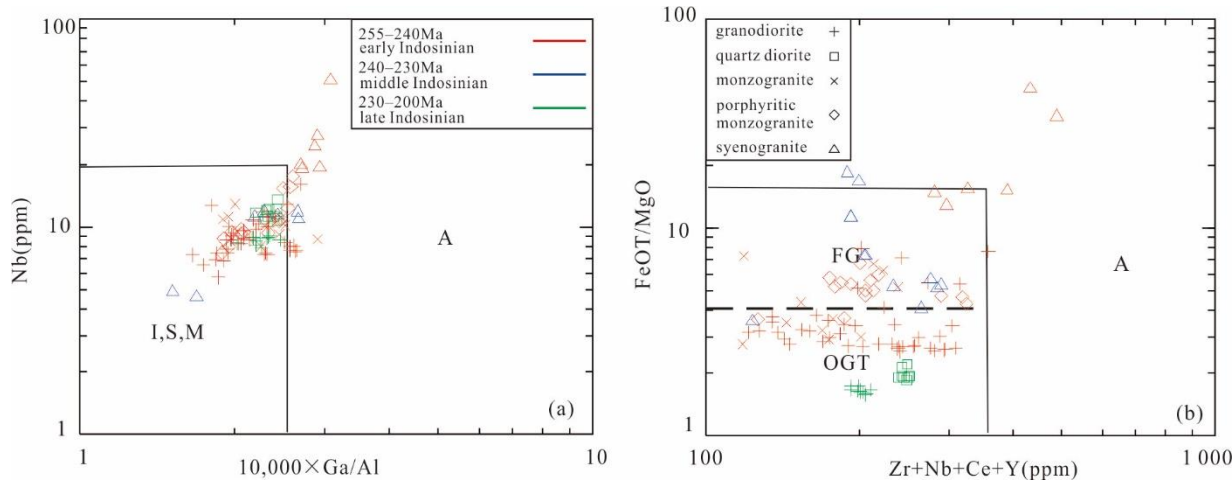


Figure 6. Diagrams of (a) $10,000 \times \text{Ga}/\text{Al}$ vs. Nb and (b) $(\text{Zr} + \text{Nb} + \text{Ce} + \text{Y})$ vs. FeOT/MgO , for the Indosian granite in the eastern region of the EKO (after [45]). FG = fractionated granites; OGT = unfractionated M-, I-, and S-type granites.

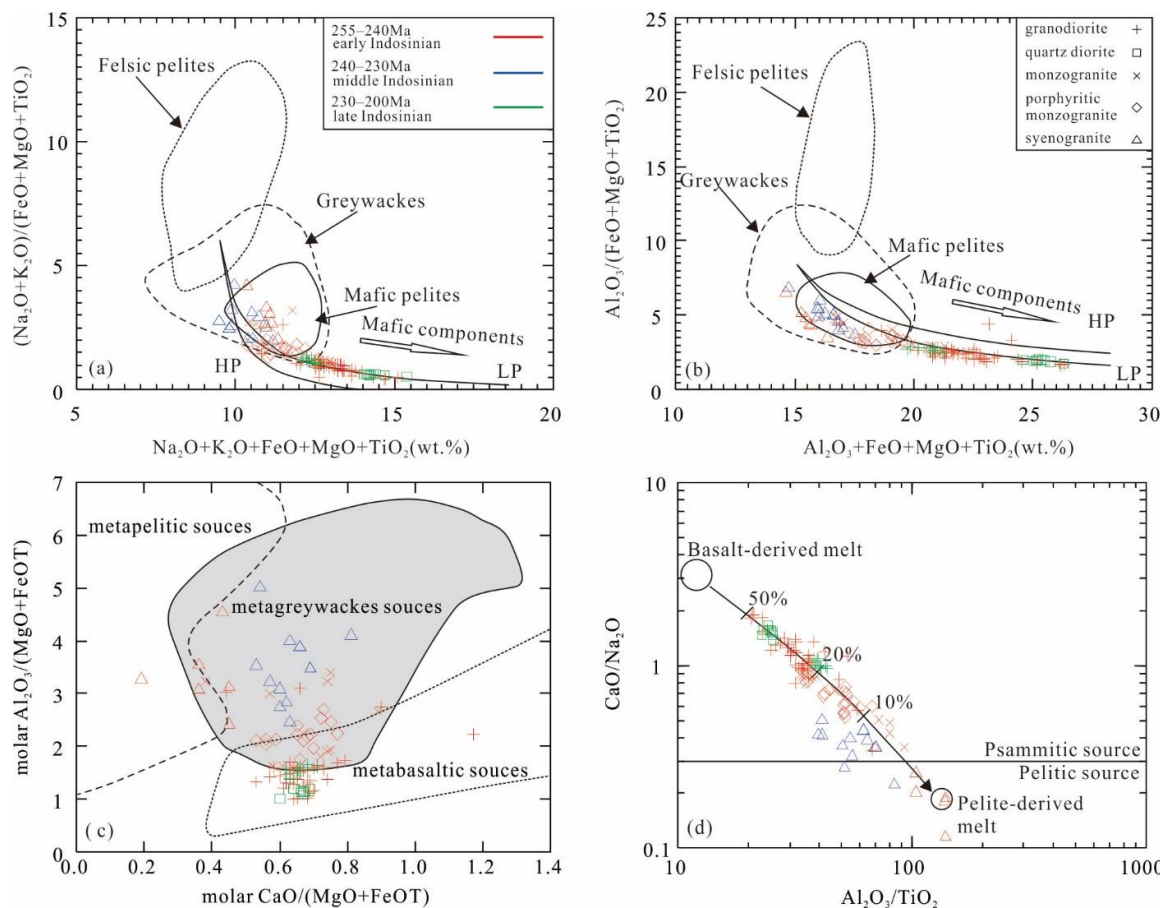


Figure 7. Diagrams of (a) $\text{Na}_2\text{O} + \text{K}_2\text{O} + \text{FeO} + \text{MgO} + \text{TiO}_2$ vs. $(\text{Na}_2\text{O} + \text{K}_2\text{O})/(\text{FeO} + \text{MgO} + \text{TiO}_2)$ (after [57]); (b) $\text{Al}_2\text{O}_3 + \text{FeO} + \text{MgO} + \text{TiO}_2$ vs. $\text{Al}_2\text{O}_3/(\text{FeO} + \text{MgO} + \text{TiO}_2)$ (after [57]); (c) molar $\text{CaO}/(\text{MgO} + \text{FeOT})$ vs. molar $\text{Al}_2\text{O}_3/(\text{MgO} + \text{FeO})$ (after [58]); and (d) $\text{Al}_2\text{O}_3/\text{TiO}_2$ vs. $\text{CaO}/\text{Na}_2\text{O}$ (after [52]) for the Indosian granite in the eastern region of the EKO.

Furthermore, the late Paleozoic-early Mesozoic mafic magmas and granites in the EKO have similar trends [20]. The transition from a middle- to high-K calc-alkaline composition indicates that fluid metasomatism in the mantle became progressively stronger from early- to late-phase subduction. Therefore, the granite was probably derived from the partial melting of juvenile mafic low crust. The monzogranite, porphyry monzogranite, and syenogranite have high SiO_2 and Al_2O_3 contents, low $\text{CaO}/\text{Na}_2\text{O}$ ratios, and high $\text{Al}_2\text{O}_3/\text{TiO}_2$ ratios, indicating that the material in the source area may have been a greywacke (Figure 7).

5.3. Petrogenesis

The origin of granitic rocks is complex, and it mainly includes the fractional crystallization of mafic magmas [8], partial melting of subducted oceanic crust [59,60], dehydration melting of hydrous minerals [61], partial melting of the lower crust by underplating mantle-derived magma [62], and water-induced partial melting [7].

Some of the Indosinian granodiorites, monzogranites, and porphyry monzogranites in the eastern EKO contain MME (Table 1). With the evolution of the magmas from basic to felsic, the MMEs in the plutons decrease in volume. In contrast, the syenogranites contain few MME, or no MME, with the exception of the Wutuo and Keri plutons. There are no MMEs in the Kekeearlong quartz diorite. Therefore, mafic magma contributed to the formation of most of the Indosinian granites, which may be related to the fractional crystallization of mafic magma. However, the Indosinian magmatic rocks in the eastern EKO are dominated by granitic rocks [1,63], with only a small amount of mafic magmatic rocks present, so the fractional crystallization of mafic magma would not explain the petrogenesis of the Indosinian granitoids.

Adakitic magmatic rocks formed by partial melting of subducted oceanic crust have relatively low Y and Yb contents, high Sr contents, and high La/Yb , Sr/Y ratios [64,65]. The Indosinian Helegangxilikete and Kekeearlong plutons resemble adakitic magmatic rocks (Table 2, Figure 8a,b). Therefore, the plutons may be the result of the partial melting of subducted oceanic crust. However, the melt formed by partial melting of subducted oceanic crust has a lower K_2O content and lower Nb/U ratios. The results shown in the SiO_2 - K_2O diagram (Figure 3b) also indicate a probable lower crustal source for the two plutons. Moreover, the sedimentary records indicate that the EKO evolved into a continental tectonic setting during the Late Triassic [66,67]. The zircon U-Pb ages of the late Indosinian Helegangxilikete and Kekeearlong plutons are 225 ± 5 Ma and 218.3 ± 1.4 Ma, respectively. Therefore, these two plutons were not derived from the partial melting of oceanic crust.

Partial melting of thickened crust during a post-collisional stage is also an important way to generate adakitic magmatic rocks [68]. As the crust thickens, the density increases to be eclogite phase, which causes lithosphere break-off and subsidence. The mafic magma is generated by decompressive melting of mantle material. The rising mafic magma ultimately leads to underplating of the lower crust to form adakitic granitic magma [69–71]. Accordingly, the adakitic Helegangxilikete and Kekeearlong plutons are probably related to the partial melting of the thickened lower crust during a post-collisional stage of an orogenic cycle.

Table 2. Petrogeochemical characteristics of the Indosinian granite in eastern region of EKO.

| Locality | Rock | SiO ₂ (wt.%) | Sr (ppm) | Y (ppm) | Sr/Y | Rb/Sr | La/Yb | Yb/Lu | 10,000 × Ga/Al | Nb/Ta | A/CNK | δ Eu | Mg [#] | T (°C) | |
|------------------|--------------------------|-------------------------|------------------------|------------------------|------------------------|------------------------|------------------------|------------------------|---------------------|------------------------|------------------------|---------------------|---------------------|------------------|------------------|
| Halagatu | granodiorite | 65.31–68.45 (67.19) | 224–353 (268) | 17.10–25.10 (21.38) | 10.42–20.47 (12.84) | 0.25–0.53 (0.42) | 5.99–15.77 (11.59) | 5.74–6.63 (6.24) | 1.85–2.21 (2.01) | 8.79–12.31 (10.34) | 0.93–1.02 (0.98) | 0.82–1.00 (0.89) | 32–39 (36) | 699–755 (714) | |
| | monzogranite | 72.63–73.01 (72.88) | 172–179 (176) | 15.00–19.30 (16.47) | 9.27–11.79 (10.84) | 0.82–0.91 (0.87) | 12.23–17.18 (14.75) | 5.33–6.20 (5.70) | 1.91–2.01 (1.96) | 9.03–10.90 (10.11) | 1.03–1.05 (1.04) | 0.64–0.72 (0.68) | 21–26 (23) | 772–784 (36) | |
| | porphyritic monzogranite | 69.87–73.46 (71.47) | 172–234 (195) | 12.50–21.80 (17.68) | 8.41–15.70 (11.36) | 0.53–0.74 (0.63) | 11.44–18.46 (14.55) | 6.14–6.97 (6.42) | 1.90–2.09 (2.01) | 8.05–12.12 (10.63) | 1.00–1.05 (1.03) | 0.88–1.09 (0.97) | 21–28 (25) | 744–769 (760) | |
| | syenogranite | 74.02–74.87 (74.53) | 74.2–93.3 (83.77) | 70.60–80.60 (76.20) | 0.96–1.32 (1.11) | 1.84–2.01 (1.97) | 4.82–5.28 (5.12) | 6.61–6.76 (6.67) | 2.88–3.08 (2.95) | 11.72–12.89 (12.23) | 0.99–1.01 (1.00) | 0.48–0.50 (0.48) | 4–11 (6) | 805–827 (816) | |
| | granodiorite | 64.52–68.59 (66.88) | 164–332 (256) | 16.30–25.00 (19.26) | 8.96–19.64 (13.59) | 0.35–0.55 (0.42) | 4.97–21.31 (12.05) | 5.58–6.67 (6.11) | 1.91–2.54 (2.21) | 6.02–13.33 (10.16) | 0.96–1.03 (0.98) | 0.74–1.13 (0.85) | 30–42 (39) | 688–784 (746) | |
| Wutuo | porphyritic monzogranite | 70.60–72.58 (71.85) | 183–205 (195) | 24.70–27.50 (25.77) | 6.65–8.30 (7.60) | 0.82–1.01 (0.93) | 11.11–11.83 (11.44) | 5.98–6.06 (6.01) | 2.49–2.60 (2.56) | 7.50–10.27 (9.28) | 0.99–1.02 (1.00) | 0.49–0.53 (0.52) | 28–30 (29) | 790–801 (797) | |
| | syenogranite | 75.38–76.27 (75.59) | 18.2–30.8 (26.13) | 21.50–28.00 (24.70) | 0.85–1.25 (1.05) | 7.28–10.88 (8.62) | 8.33–10.13 (9.09) | 6.16–6.53 (6.33) | 2.70–2.94 (2.79) | 10.84–12.69 (11.53) | 1.01–1.08 (1.04) | 0.14–0.23 (0.18) | 11–13 (12) | 803–812 (808) | |
| | syenogranite | 66.60–72.86 (69.73) | 102–140 (121) | 14.00–18.00 (16.00) | 7.29–7.78 (7.53) | 1.65–2.58 (2.11) | 40.85–59.24 (50.05) | 6.88–7.08 (6.98) | 1.81–2.70 (2.26) | 14.43–19.75 (17.09) | 0.98–1.07 (1.03) | 0.21–0.23 (0.22) | 19–35 (27) | 773–815 (794) | |
| | monzogranite | 67.58–73.19 (69.16) | 392–496 (448) | 8.96–12.30 (11.07) | 35.64–50.33 (40.78) | 0.18–0.27 (0.24) | 15.97–24.32 (20.46) | 5.77–7.00 (6.61) | 2.25–2.92 (2.46) | 9.40–13.00 (11.16) | 0.98–1.05 (1.00) | 0.95–1.30 (1.07) | 17–40 (33) | 701–756 (728) | |
| Xiangjiananshan | porphyritic monzogranite | 68.72–72.16 (70.23) | 359–436 (393) | 9.76–13.40 (11.52) | 28.13–41.09 (34.63) | 0.25–0.35 (0.3) | 14.27–33.4 (26.41) | 5.89–6.87 (6.46) | 2.34–2.55 (2.45) | 9.52–14.52 (11.70) | 0.98–1.02 (1.01) | 0.92–1.05 (0.98) | 25–33 (29) | 722–742 (736) | |
| | Qushiang | granodiorite | 60.26–65.88 (63.19) | 350–518 (421) | 17.51–21.12 (19.50) | 18.87–25.52 (21.53) | 0.17–0.95 (0.11) | 13.51–34.02 (18.93) | 5.40–6.37 (6.18) | 2.29–2.65 (2.50) | 13.38–26.88 (18.81) | 0.92–0.99 (0.94) | 0.47–0.50 (0.49) | 40–44 (43) | 562–790 (749) |
| | Chaochuolutaogai | granodiorite | 65.27–74.25 (67.51) | 103–293 (203) | 9.27–26.10 (17.81) | 4.79–22.65 (13.21) | 0.12–1.60 (0.59) | 11.10–49.43 (23.77) | 6.28–6.69 (6.52) | 1.66–1.94 (1.91) | 9.40–19.17 (14.46) | 0.91–1.06 (1.00) | 0.51–1.02 (0.77) | 20–28 (25) | 740–788 (772) |
| Chahantaolegai | syenogranite | 71.52–74.90 (73.75) | 33.6–127 (77.13) | 3.95–9.39 (7.44) | 3.58–32.10 (12.84) | 0.77–5.51 (2.03) | 23.48–40.22 (31.80) | 5.29–6.58 (6.08) | | 9.36–18.22 (15.37) | 1.05–1.13 (1.10) | 0.27–0.52 (0.40) | 10–36 (19) | 743–786 (771) | |
| | Keri | syenogranite | 72.06–74.49 (73.39) | 71–211 (141) | 7.45–14.83 (11.12) | 8.10–18.44 (12.68) | 0.35–1.24 (0.75) | 10.68–39.71 (21.72) | 5.55–6.46 (6.04) | 0.85–2.67 (2.04) | 15.43–27.85 (18.84) | 1.00–1.13 (1.06) | 0.29–0.51 (0.38) | 15–33 (26) | 689–818 (785) |
| Helegangxilikete | granodiorite | 67.12–69.28 (68.04) | 348–434 (390) | 8.94–11.60 (10.17) | 34.46–43.40 (38.41) | 0.27–0.39 (0.32) | 21.91–36.02 (27.15) | 5.68–7.00 (6.22) | 2.03–2.46 (2.26) | 10.29–13.82 (12.21) | 0.95–0.98 (0.96) | 0.95–1.08 (1.00) | 52–55 (54) | 747–758 (754) | |
| Kekeealong | quartz diorite | 60.08–62.69 (62.04) | 395–485 (435) | 12.50–15.60 (13.90) | 27.30–38.80 (31.58) | 0.14–0.19 (0.16) | 17.59–27.43 (23.51) | 6.94–7.64 (7.32) | 2.21–2.43 (2.35) | 16.19–21.84 (19.03) | 0.92–0.98 (0.94) | 0.93–1.01 (0.97) | 46–51 (49) | 753–764 (758) | |

atomic Mg[#] = 100 × (Mg²⁺ / (Mg²⁺ + TFe²⁺)); δEu = √Eu_N / (Sm_N × Gd_N); T (°C) = 12,900 / [LnDz + 0.85 × M + 2.95] – 273.15 [72]; data in () are average

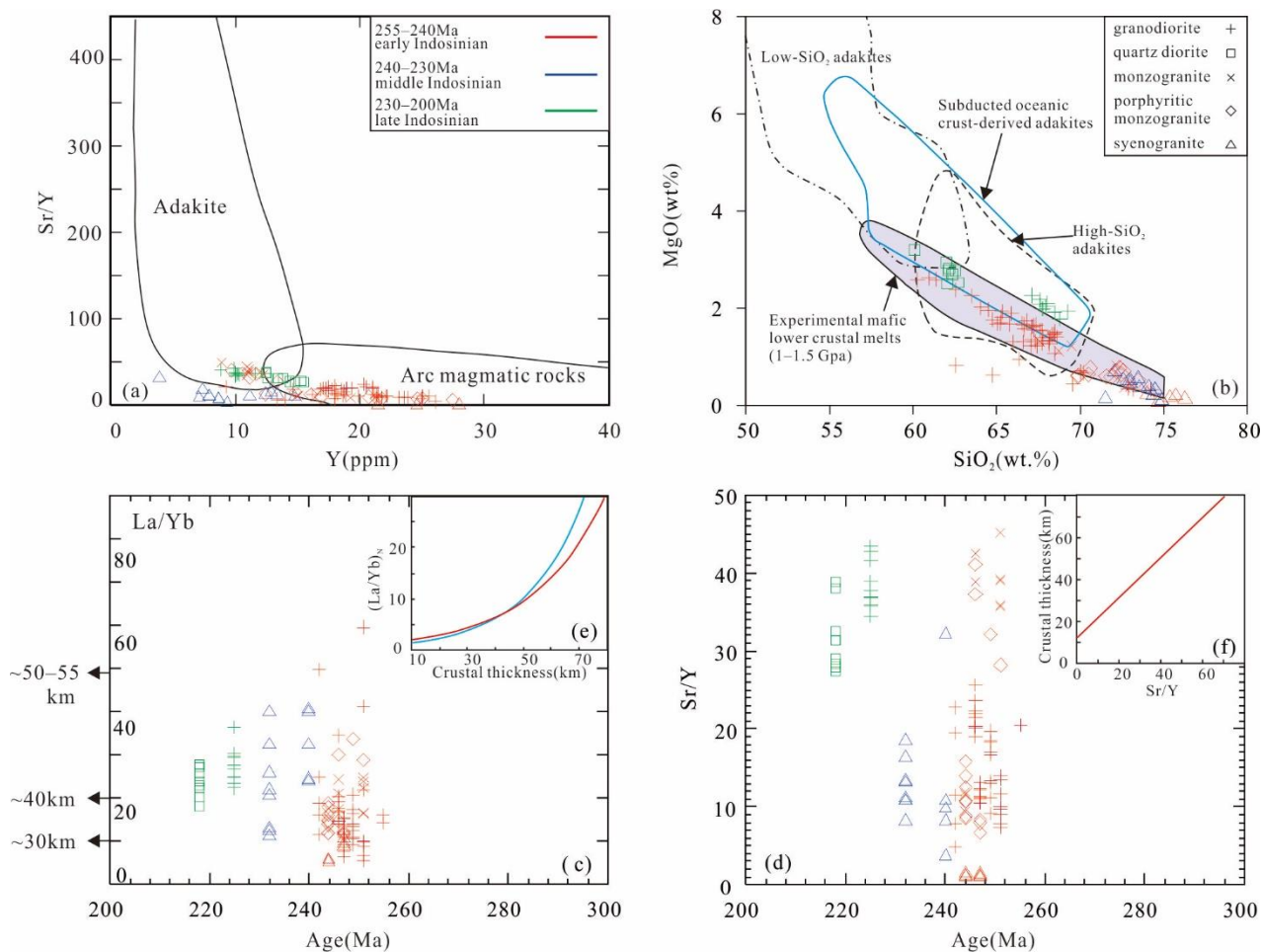


Figure 8. Diagrams of (a) Sr/Y vs. Y ; (b) MgO vs. SiO_2 ; (c) La/Yb vs. ages; and (d) Sr/Y vs. ages for the granite plutons in the eastern region of the EKO during the Indosinian (a after [69]; b after [69]); (e) Diagram of $(\text{La}/\text{Yb})_N$ vs. crustal thickness (after [73]); (f) Crustal thickness vs. Sr/Y (after [73]).

Compared to other rocks generated from the melting of continental crust, the Helegangxilikete, Kekeearlong, and Qushiang plutons have high $\text{Mg}^{\#}$ values and are indicative of mantle source characteristics (Figure 9) [59,60]. Granitic rocks with compositions similar to mantle material can be attributed to fractional crystallization of mantle source magma [69], crust–mantle magma mixing [74], or delamination of the crustal metasomatic mantle [75]. As mentioned above, only a small amount of mafic magma emplacement occurred in the EKO during the Indosinian, so the fractional crystallization of mantle magma cannot explain the high $\text{Mg}^{\#}$ values of these three plutons. Macroscopically, MMEs are evidence of crust–mantle magmatic mixing. The Helegangxilikete and Qushiang plutons contain MMEs, with the magma mixing phenomenon common in the granitoids of the EKO. Therefore, the high $\text{Mg}^{\#}$ values may be related to the magma mixing of mantle–derived and crust–derived melts. However, studies have shown that the mafic magma had a high temperature. When mafic magma mixes with the host felsic magma, the physical properties of the mafic magma and the felsic magma are different due to temperature differences. Generally, the material in the host magma can enter the MMEs easily, while the enclave material appears to have difficulty entering the host magma [76]. Therefore, the mantle source characteristics of host rocks can be explained by the homogeneous mixing of mantle source magma and host rocks in the deep crust. The Kekeearlong pluton has a high $\text{Mg}^{\#}$ value but does not contain MMEs. The adakitic nature and high $\text{Mg}^{\#}$ value of the Kekeearlong pluton may result from partial melting of the lower crust during delamination–related metasomatism in the mantle [77].

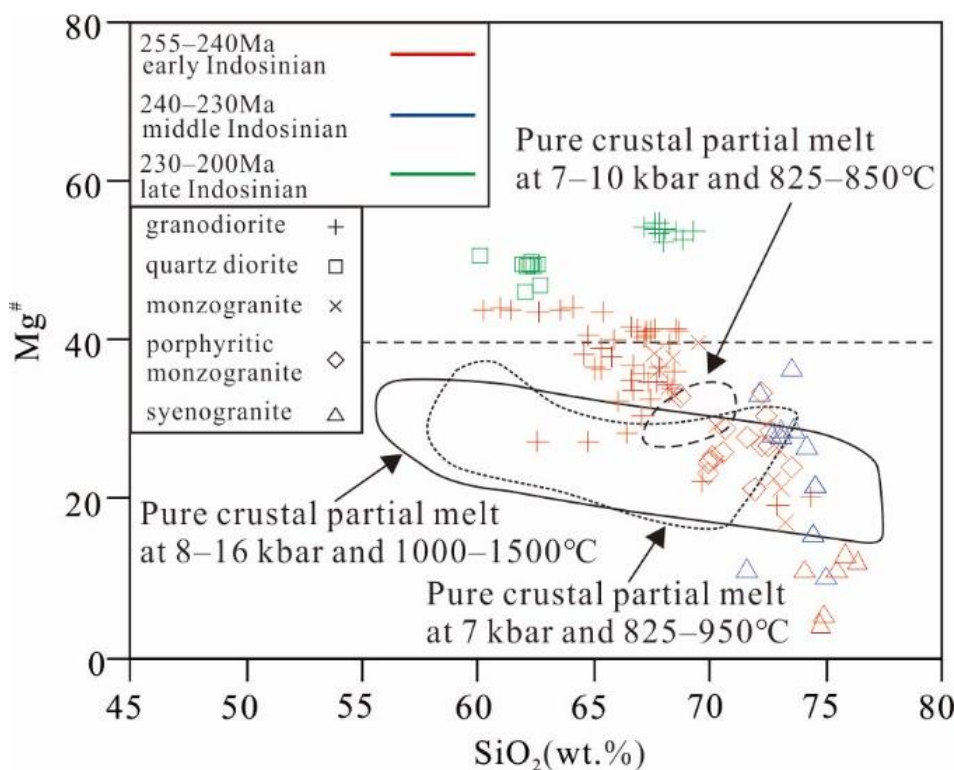


Figure 9. Diagrams of $Mg^{\#}$ vs. SiO_2 for the Indosinian granite plutons in the eastern region of the EKO. The results of the published work shown in the figure include the fields of pure crustal partial melts determined in experimental studies for dehydration melting of a two-mica schist at 7–10 kbar and temperatures of 825–850 °C [78]; the dehydration melting of low-K basaltic rocks at 8–16 kbar and temperatures of 1000–1050 °C [59]; moderately hydrous (1.7–2.3% H_2O) medium- to high-K basaltic rocks at 7 kbar and temperatures of 825–950 °C [51].

Granitic magma can be formed by dehydration partial melting of hydrous minerals (e.g., muscovite, biotite, and amphibole). Studies have shown that the dehydration partial melting temperature of muscovite is roughly 650–750 °C under medium-pressure conditions [79], while the dehydration partial melting temperature of biotite and hornblende in "dry" conditions is above 800 °C [3,80,81]. The zircon saturation temperature of Indosinian granodiorite, monzogranite, and porphyritic monzogranite in the EKO was below 800 °C (average 749 °C) (Figure 10). In contrast, the lower K/Na and Rb/Sr ratios are different from those of the melt formed by the dehydration partial melting of muscovite. Therefore, the dehydration partial melting of hydrous minerals cannot explain the petrogenesis of these rocks. Previous studies show that the melting temperature of metabasalts can be reduced to 700–750 °C by adding water under high pressure [82]. The formation of the Indosinian granodiorite, monzogranite, and porphyry monzogranite in the EKO may, therefore, be related to water-induced partial melting [7]. In the subduction and post-collisional stages, the large-scale underplating of mantle-derived magma provides both heat and water for the partial melting of source rocks. Especially, the influx of water significantly reduces the melting point of rocks in the source area, leading to the generation of granitic magma. The differences in these granitic rocks are not only related to the heterogeneity of the source area but also closely related to the water content in the source area [83]. For the Indosinian granites in the EKO, the Chahantaolegai syenogranite had a relatively low zircon saturation temperature of 771 °C on average (Figure 10), similar to that of dehydration melting for muscovite. In addition, the pluton has high K/Na and Rb/Sr ratios, indicating that it was generated (at least in part) from dehydration melting of muscovite. By comparison, the Keri, Halagatu, and Wutuo syenogranite had relatively high crystallization temperatures of 800 °C, higher than the dehydration partial melting temperature of biotite and amphibole.

They have low K/Na and Rb/Sr ratios, similar to the melt formed by dehydration partial melting of biotite or amphibole [84]. In addition, these Indosian granitoids are similar to the melt formed during a water-unsaturated (2%–5%) melting experiment at 800–900 °C and 3–10 kbar conditions (Figure 11) [62], which shows that the melt was unsaturated at the initial melting stage. Accordingly, the formation of the Indosian granitoids in the EKO is closely related to the temperature and the water content of the source region.

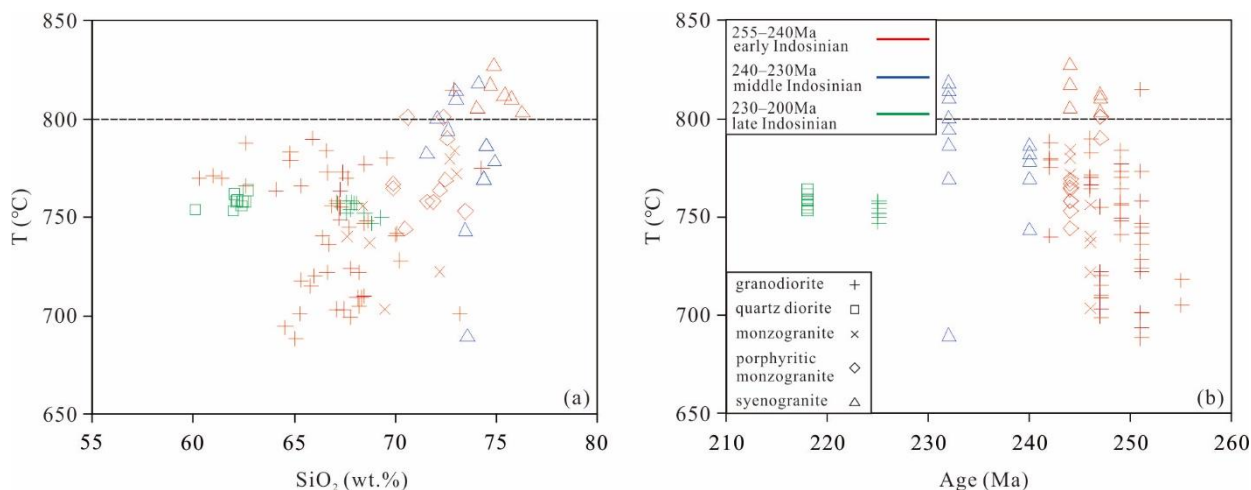


Figure 10. Diagrams of (a) T vs. SiO₂ and (b) T vs. age for the Indosian granite plutons in the eastern region of the EKO.

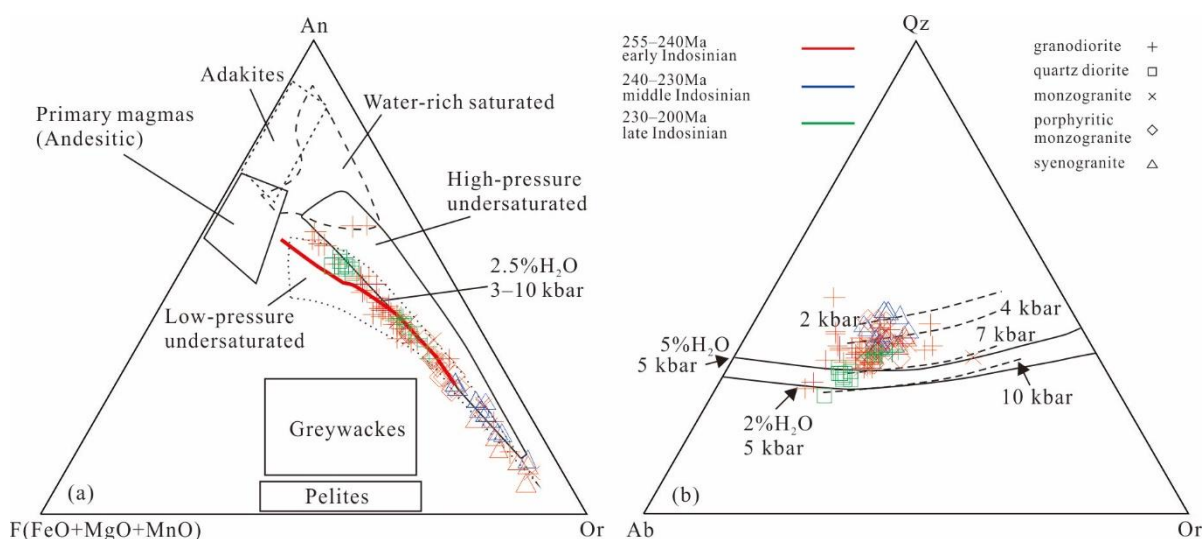


Figure 11. Diagrams of (a) F (FeO + MgO + MnO)–An–Or [60] and (b) Ab–Qz–Or (solid lines after [85]; dashed lines after [86]) for the Indosian granite in the eastern region of the EKO. Qz = quartz, An = anorthite, Ab = albite, and Or = orthoclase.

6. Tectonic Setting of the Granitoids

The Indosian was an important transition period of tectonic settings for the eastern EKO [14,87–89]. These settings included ocean subduction, continent–continent collision, and post-collisional stages. In such a complex geodynamic background, the physicochemical environment and crustal properties of the EKO changed in response to the prevailing tectonic setting, thus affecting the composition, distribution, and genesis of granites in the EKO during this period.

In the early Indosian (>252–240 Ma), the magmatic activity in the eastern EKO was very intense, resulting in large granitic batholiths that are primarily exposed in the

region (e.g., Wutuo pluton, Xiangjiananshan pluton, and Halagatu pluton). The granitoids were mainly distributed in an East–West trend, primarily concentrated within the CKB [19,20,90,91]. The main rock type in the EKO is granodiorite, which typically has a medium K calc-alkaline composition (Figure 3b). It is enriched in LILEs (e.g., Rb and U), but depleted in HFSEs, and has a composition similar to arc magmas. In the tectonic discriminant diagram, the granodiorite has a composition consistent with slab failure area and arc-related magmatic rock (Figure 12). The intense magmatic activity in the eastern EKO during the early Indosinian may have been controlled by slab break-off (Figure 13a). As a result of the continuous subduction of the northern Paleo-Tethys Ocean, the density of the oceanic crust probably increased, reaching a density comparable to that of eclogite. This increase in density would have caused the subducted oceanic crust to break-off and sink, resulting in rapid upwelling and decompression of the mantle to form mafic magma [18,48]. At the same time, a large amount of water rose into the lower crust, reducing the melting temperature of the source rocks, and resulting in the development of granitic rocks in the EKO.

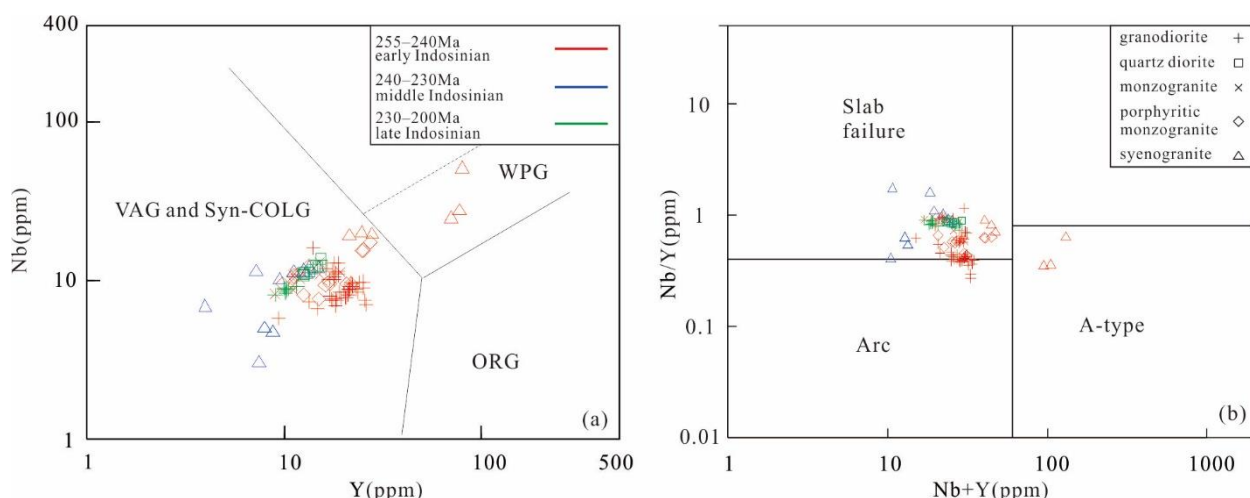


Figure 12. Diagrams of the tectonic setting for the Indosinian granite in the eastern region of the EKO ((a), after [92,93]; (b), after [94]). WPG = within plate granites; VAG = volcanic arc granites; ORG = ocean ridge granite; syn-COLG = syn-collision granite.

In the middle Indosinian (240–230 Ma), the magmatic activity was very weak, evidenced by the limited number of plutons in the eastern EKO (e.g., Keri and Chahantaolegai plutons). Large-scale fault zones mostly control the distribution of plutons, mainly outcropped near fault zones. The weakening of magmatic activity was likely related to the collision between the Bayan Har/Qiangtang and East Kunlun blocks (Figure 13b). Due to this continent–continent collision, the EKO would have been in a collisional setting at the time, which is not conducive to the formation of magma, but rather a decrease in magmatic activity [48,95–97].

In the late Indosinian (230–205 Ma), there were magmatic flare-ups, but the composition of the magma was different from that of the early Indosinian magmatic rocks. The compositions are mostly granodioritic and monzogranitic, and distributed throughout the EKO. Compared with the early Indosinian, the outcrop size of the late Indosinian granitoids is relatively small. They generally intrude into the early plutons and sedimentary strata as small plutons, stocks, and dikes. The granites of late Indosinian evolved from medium- to high-K calc-alkaline compositions (Figure 3b), with characteristics typical of post-collisional magmatic rocks [98,99]. In addition, these magmatic rocks cut across the structural trend of the orogen, indicative of a post-collision setting. In the tectonic setting discrimination diagram, magmatic rocks also have compositions similar to those associated with intraplate environments (Figure 12). The Helegangxilikete and Kekeearlong plutons

have the characteristics of adakitic magmatic rocks. In addition, A-type granites intruded into the EKO during this period, indicating that the EKO has already been in an extensional tectonic setting caused by the delamination of the thickened lower crust [100–102].

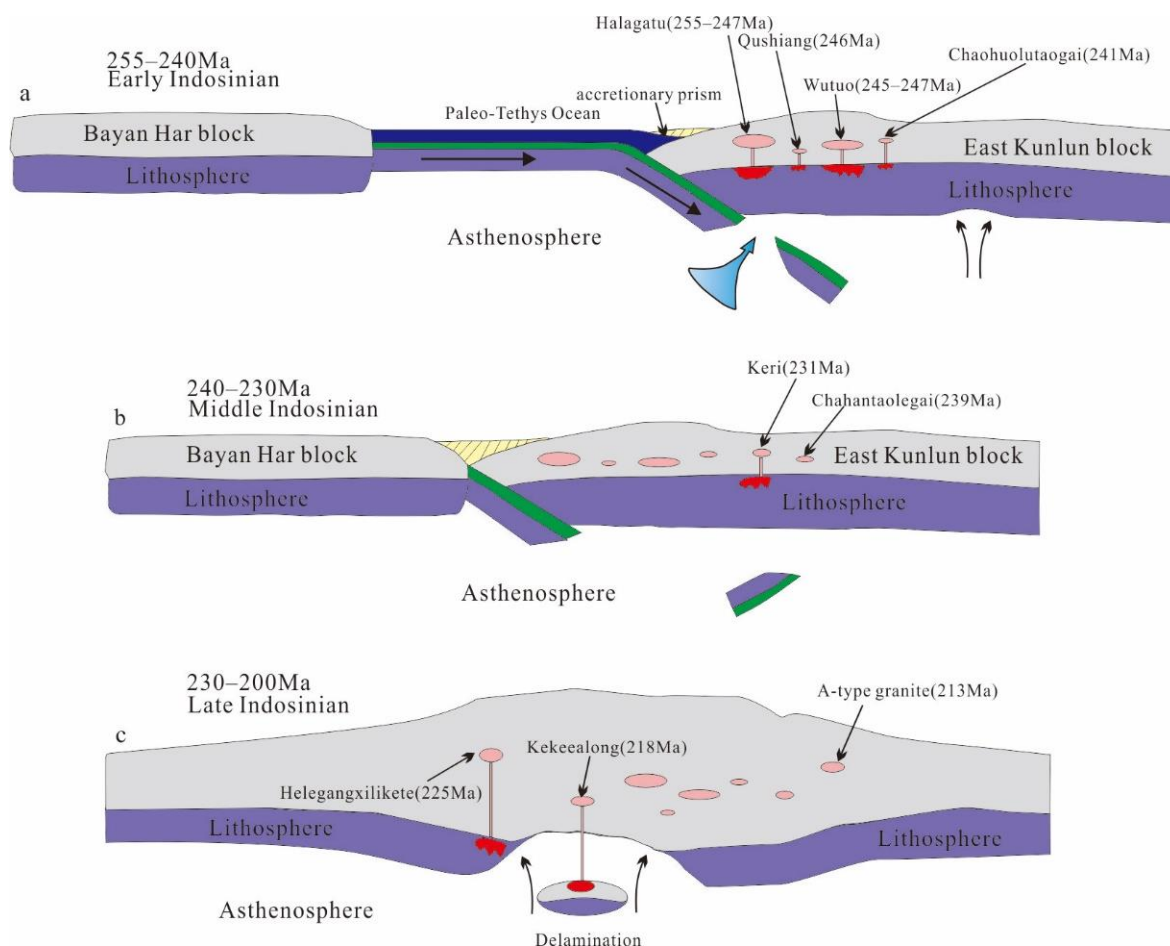


Figure 13. Diagram showing the tectonic setting of the Indosinian magmatism in the EKO. (a) Subduction stage: As a result of break-off of the subducted slab, the mafic magma underplated the lower crust and formed the early Triassic arc magmatic rocks in the EKO; (b) Collision stage: Collision between the Bayan Har block with the East Kunlun block. The granite was derived from muscovite and either biotite or hornblende during dehydration partial melting; (c) Post-collision: The delamination of thickened crust resulted in an extensional setting, where mafic magma underplated the lower crust to form granite.

Studies show that the Sr/Y and La/Yb ratios of granites are good indicators of changes to crustal thickness in orogenic belts [73]. From the early Indosinian to the late Indosinian, the Sr/Y and La/Yb ratios of the granitoids in the EKO gradually increased, indicating that the crustal thickness continuously increased during the Indosinian (Figure 8c,d). The delamination of the thickened crust probably caused the upwelling of the asthenosphere, which would have provided a source of heat for the partial melting of the rock, and provided a channel for the migration of fluids, which would have led to a significant increase in magmatic activity in this stage of the orogenic process (Figure 13c).

7. Conclusions

- Most early Indosinian to late Indosinian granitoids occur in the eastern EKO, consisting of granodiorite, monzogranite, porphyry monzogranite, and syenogranite. The granitoids geochemically evolved from medium- to high-K calc-alkaline in composition.

- (2) In the early Indosinian, the break-off of the northern Paleo-Tethys Ocean resulted in the rapid upwelling of the mantle and decompression-related formation of mafic magma. At the same time, a large amount of water entered the lower crust, reducing the melting temperature of the source rocks, and forming a large volume of granitic rocks.
- (3) During the middle Indosinian, the collision of the Bayan Har and East Kunlun blocks was an unfavorable environment for the development of fissures and, consequently, the movement of fluids into the crust in the EKO. The formation of magma could be attributed to dehydration partial melting of hydrous minerals.
- (4) In the late Indosinian, the delamination of the thickened lower crust resulted in the upwelling of the asthenosphere, providing heat for the partial melting of rocks, but also provided a channel for the migration of fluids, which led to magmatic flare-ups during the post-collision stage.

Supplementary Materials: The following supporting information can be downloaded at: <https://www.mdpi.com/article/10.3390/min12121604/s1>, Table S1: Whole-rock major element (wt.%) and trace element (ppm) compositions for the Indosinian granites in eastern region of East Kunlun.

Author Contributions: Conceptualization, G.C. and X.P.; investigation, Z.L., Y.C., C.L. and L.P.; writing—original draft preparation, G.C.; writing—review and editing, G.C., X.P. and R.L.; funding acquisition, X.P. and G.C. All authors have read and agreed to the published version of the manuscript.

Funding: This research was funded by the National Natural Science Foundation of China (Grant Nos. 42172236, 41872233, and 41872235); the development fund project of MNR Key Laboratory of Metallogeny and Mineral Assessment (Grant No. Z006); Key R&D and promotion projects in Henan Province (212102310030); the Interdisciplinary Sciences Project, Nanyang Institute of Technology.

Data Availability Statement: The original contributions presented in the study are included in the article/Supplementary Material.

Acknowledgments: We are grateful to the journal editor and Gaoxue Yang for their suggestions, which helped in improving our manuscript. We also thank the four anonymous referees for their constructive reviews and suggestions.

Conflicts of Interest: The authors declare no conflict of interest.

References

1. Mo, X.X.; Luo, Z.H.; Deng, J.F.; Yu, X.G.; Liu, C.D.; Shen, H.W.; Yuan, W.M.; Liu, Y.H. Granitoids and Crustal Growth in the East-Kunlun Orogenic Belt. *J. China Univ. Geosci.* **2007**, *13*, 403–414.
2. Clemens, J.D.; Stevens, G. What controls chemical variation in granitic magmas? *Lithos* **2012**, *134–135*, 317–329. [[CrossRef](#)]
3. Brown, M. Granite: From genesis to emplacement. *Bull. Geol. Soc. Am.* **2013**, *125*, 1079–1113. [[CrossRef](#)]
4. Wu, F.Y.; Liu, X.C.; Ji, W.Q.; Wang, J.M.; Yang, L. Highly fractionated granites: Recognition and research. *Sci. China Ser. D.* **2017**, *47*, 745–765. [[CrossRef](#)]
5. Clemens, J.D. Granitic magmas with I-type affinities, from mainly metasedimentary sources: The Harcourt batholith of southeastern Australia. *Contrib. Mineral. Petrol.* **2018**, *173*, 93–113. [[CrossRef](#)]
6. Davidson, J.; Turner, S.; Handley, H.; Macpherson, C.; Dosseto, A. Amphibole "sponge" in arc crust? *Geology* **2007**, *35*, 787–790. [[CrossRef](#)]
7. Weinberg, R.F.; Hasalová, P. Water-fluxed melting of the continental crust: A review. *Lithos* **2015**, *212–215*, 158–188. [[CrossRef](#)]
8. Gao, P.; Zheng, Y.F.; Zhao, Z.F. Experimental melts from crustal rocks: A lithochemical constraint on granite petrogenesis. *Lithos* **2016**, *266–267*, 133–157. [[CrossRef](#)]
9. Li, X.H.; Li, Z.X.; Li, W.X.; Liu, Y.; Yuan, C.; Wei, G.J.; Qi, C.S. U–Pb zircon, geochemical and Sr–Nd–Hf isotopic constraints on age Guangdong, SE China: A major igneous event in response to foundering of a subducted flat-slab? *Lithos* **2007**, *96*, 186–204. [[CrossRef](#)]
10. Xiao, Q.H.; Deng, J.F.; Qiu, R.Z.; Liu, Y.; Feng, Y.F. A preliminary study of the relationship between granitoids and the growth of continental crust: A case study of the formation of key orogen granitoids in China. *Geol. China* **2009**, *36*, 594–622.
11. Wang, T.; Wang, X.X.; Guo, L.; Zhang, L.; Tong, Y.; Li, S.; Huang, H.; Zhang, J.J. Granitoid and tectonics. *Acta. Petrol. Sin.* **2017**, *35*, 1459–1478.
12. Zhu, D.C.; Zhao, Z.D.; Niu, Y.L.; Mo, X.X.; Chung, S.L.; Hou, Z.Q.; Wang, L.Q.; Wu, F.Y. The Lhasa Terrane: Record of a microcontinent and Its histories of drift and growth. *Earth Planet. Sci. Lett.* **2011**, *301*, 241–255. [[CrossRef](#)]

13. Luo, Z.H.; Ke, S.; Cao, Y.Q.; Deng, J.F.; Shen, H.W. Indosinian mantle-derived magmatism in the East Kunlun. *Geol. Bull. China* **2002**, *21*, 292–297.
14. Ma, C.Q.; Xiong, F.H.; Zhang, J.Y.; Liu, B.; Huang, J.; Jiang, H.A. The Effects of Subduction Plate of Magmatism in the Stage of Plate Subduction to Post-Tectonic: Evidence of Mafic Dike of Early Permian–Late Triassic East Kunlun. *Acta Geol. Sin.* **2013**, *87*, 79–81.
15. Ma, C.Q.; Xiong, F.H.; Yin, S.; Wang, L.X.; Gao, K. Intensity and cyclicity of orogenic magmatism: An example from a Paleo-Tethyan granitoid batholith, Eastern Kunlun, northern Qinghai–Tibetan Plateau. *Acta Geol. Sin.* **2015**, *31*, 3555–3568.
16. Meng, F.C.; Zhang, J.X.; Cui, M.H. Discovery of Early Paleozoic eclogite from the East Kunlun, Western China and its tectonic significance. *Gondwana Res.* **2013**, *23*, 825–836. [CrossRef]
17. Yu, M.; Feng, C.Y.; Santosh, M.; Mao, J.W.; Zhu, Y.F.; Zhao, Y.M.; Li, D.X.; Li, B. The Qiman Tagh Orogen as a window to the crustal evolution in northern Qinghai–Tibet Plateau. *Earth–Sci. Rev.* **2017**, *167*, 103–123. [CrossRef]
18. Dong, Y.P.; He, D.F.; Sun, S.S.; Liu, X.M.; Zhou, X.H.; Zhang, F.F.; Yang, Z.; Cheng, B.; Zhao, G.C.; Li, J.H. Subduction and Accretionary Tectonics of the East Kunlun Orogen, Western Segment of the Central China Orogenic System. *Earth–Sci. Rev.* **2018**, *186*, 231–261. [CrossRef]
19. Li, R.B.; Pei, X.Z.; Pei, L.; Li, Z.C.; Chen, G.C.; Chen, Y.X.; Liu, C.J.; Wang, M. The Early Triassic Andean-type Halagatu granitoids pluton in the East Kunlun orogen, northern Tibet Plateau: Response to the northward subduction of the Paleo-Tethys Ocean. *Gondwana Res.* **2018**, *62*, 212–226. [CrossRef]
20. Chen, G.C.; Pei, X.Z.; Li, R.B.; Li, Z.C.; Pei, L.; Liu, C.H.; Chen, Y.X.; Li, X.B. Triassic magma mixing and mingling at the eastern section of Eastern Kunlun: A case study from Xiangjiananshan granitic batholith. *Acta Petrol. Sin.* **2018**, *34*, 2441–2480.
21. Li, R.B.; Pei, X.Z.; Li, Z.C.; Pei, L.; Chen, G.C.; Chen, Y.X.; Liu, C.J.; Wang, M. Paleo-Tethys Ocean subduction in eastern section of East Kunlun Orogen: Evidence from the geochronology and geochemistry of the Wutuo pluton. *Acta Petrol. Sin.* **2018**, *34*, 3399–3421.
22. Chen, G.C.; Pei, X.Z.; Li, R.B.; Li, Z.C.; Liu, C.J.; Chen, Y.X.; Pei, L.; Wang, M.; Li, X.B. Paleo-Tethyan Oceanic Crust Subduction in the Eastern Section of the East Kunlun Orogenic Belt: Geochronology and Petrogenesis of the Qushi’ang Granodiorite. *Acta Geol. Sin.–Engl.* **2017**, *91*, 565–580. [CrossRef]
23. Chen, G.; Pei, X.Z.; Li, Z.C.; Li, R.B.; Chen, Y.X.; Liu, C.J.; Chen, G.C.; Wang, X.B.; Sang, J.Z.; Yang, S.; et al. Zircon U–Pb geochronology, geochemical characteristics and geological significance of Chaohuolutaolegai granodiorite in Balong area, East Kunlun Mountains. *Geol. Bull. China* **2016**, *35*, 1990–2005.
24. Deng, W.B.; Pei, X.Z.; Liu, C.J.; Li, Z.C.; Li, R.B.; Chen, Y.X.; Chen, G.C.; Yang, S.; Chen, G.; Sang, J.Z.; et al. LA-ICP-MS zircon U–Pb dating of the Chahantaolegai syenogranites in Xianggride area of East Kunlun and its geological significance. *Geol. Bull. China* **2016**, *35*, 687–699.
25. Chen, G.C.; Pei, X.Z.; Li, R.B.; Li, Z.C.; Liu, C.J.; Chen, Y.X.; Pei, L.; Li, X.B. Age and lithogenesis of Keri syenogranite from eastern part of East Kunlun Orogenic Belt: Constraint on the Middle Triassic tectonic evolution of East Kunlun. *Acta Petrol. Sin.* **2018**, *34*, 567–585.
26. Chen, G.C.; Pei, X.Z.; Li, R.B.; Li, Z.C.; Pei, L.; Liu, Z.Q.; Chen, Y.X.; Liu, C.J.; Gao, J.M.; Wei, F.H. Zircon U–Pb Geochronology Geochemical Characteristics and Geological Significance of Cocoe A’Long Quartz Diorites Body from the Hongshuichuan Area in East Kunlun. *Acta Geol. Sin.* **2013**, *87*, 178–196.
27. Chen, G.C.; Pei, X.Z.; Li, R.B.; Li, Z.C.; Pei, L.; Liu, Z.Q.; Chen, Y.X.; Liu, C.J. Late Triassic magma mixing in the East Kunlun orogenic belt: A case study of Helegang Xilikete granodiorites. *Geol. China* **2013**, *40*, 1044–1065.
28. Chen, G.C.; Pei, X.Z.; Li, R.B.; Li, Z.C.; Pei, L.; Liu, Z.Q.; Chen, Y.X.; Liu, C.J.; Gao, J.M.; Wei, F.H. Geochronology and genesis of Helegang Xilikete plutons from south margin of eastern part in East Kunlun Orogenic Belt and their geological significance. *Acta Geol. Sin.* **2013**, *87*, 1524–1541.
29. Li, R.B.; Pei, X.Z.; Li, Z.C.; Sun, Y.; Feng, J.Y.; Pei, L.; Chen, G.C.; Liu, C.J.; Chen, Y.X. Geochemical features, age, and tectonic significance of the Kekekete mafic–ultramafic rocks, East Kunlun Orogen, China. *Acta Geol. Sin.* **2013**, *87*, 1319–1333.
30. Li, R.B.; Pei, X.Z.; Li, Z.C.; Sun, Y.; Pei, L.; Chen, G.C.; Chen, Y.X.; Liu, C.J.; Wei, F.H. Regional tectonic transformation in East Kunlun orogenic belt in Early Paleozoic: Constraints from the geochronology and geochemistry of Helegangnaren alkali-feldspar granite. *Acta Geol. Sin.* **2013**, *87*, 333–345.
31. Pei, X.Z.; Li, R.B.; Li, Z.C.; Liu, C.J.; Chen, Y.X.; Pei, L.; Liu, Z.Q.; Chen, G.C.; Li, X.B.; Wang, M. Composition Feature and Formation Process of Buqingshan Composite Accretionary Mélange Belt in Southern Margin of East Kunlun Orogen. *Earth Sci.* **2018**, *43*, 4498–4520.
32. Song, S.G.; Bi, H.Z.; Qi, S.S.; Yang, L.M.; Allen, M.B.; Niu, Y.L.; Su, L.; Li, W.F. HP-UHP Metamorphic Belt in the East Kunlun Orogen: Final Closure of the Proto-Tethys Ocean and Formation of the Pan–North–China Continent. *J. Petrol.* **2018**, *59*, 2043–2060. [CrossRef]
33. Pei, X.Z.; Hu, N.; Liu, C.J.; Li, R.B.; Li, Z.C.; Chen, Y.X.; Pei, L.; Liu, Z.Q.; Chen, G.C.; Yang, J. Detrital Compositon, Geochemical Characteristics and Provenance Analysis for the Maerzheng Formation Sandstone in Gerizhuotuo Area, Southern Margin of East Kunlun Region. *Geol. Rev.* **2015**, *61*, 307–323.
34. Li, Z.C.; Pei, X.Z.; Li, R.B.; Pei, L.; Liu, C.J.; Chen, Y.X.; Zhang, Y.M.; Wang, M.; Xu, T. Early Ordovician island–arc-type Manite granodiorite pluton from the Buqingshan tectonic mélange belt in the southern margin of the East Kunlun Orogen: Constraints on subduction of the Proto-Tethyan Ocean. *Geol. J.* **2017**, *52*, 510–528. [CrossRef]

35. Li, R.B.; Pei, X.Z.; Li, Z.C.; Pei, L.; Chen, G.C.; Li, X.B.; Chen, Y.X.; Liu, C.J.; Wei, B.; Wang, M. Geochemistry and tectonic setting of Qingquangou forearc basalts in central tectonic mélange of East Kunlun Orogen. *Earth Sci.* **2018**, *43*, 4251–4535.
36. Zhao, X.; Fu, L.B.; Santosh, M.; Wei, J.H.; Chen, J.J. The growth and evolution of continental crust contributed by multiple sources in the East Kunlun Orogen during Early Paleozoic. *Earth-Sci. Rev.* **2022**, *233*, 104190. [[CrossRef](#)]
37. Hu, Y.; Niu, Y.L.; Li, J.Y.; Ye, L.; Kong, J.J.; Chen, S.; Zhang, Y.; Zhang, G.R. Petrogenesis and tectonic significance of the late Triassic mafic dikes and felsic volcanic rocks in the East Kunlun Orogenic Belt, Northern Tibet Plateau. *Lithos* **2016**, *254*, 205–222. [[CrossRef](#)]
38. Liu, B.; Ma, C.Q.; Huang, J.; Wang, L.X.; Zhao, S.Q.; Yan, R.; Sun, Y.; Xiong, F.H. Petrogenesis and tectonic implications of Upper Triassic appinite dykes in the East Kunlun orogenic belt, northern Tibetan Plateau. *Lithos* **2017**, *284*, 766–778. [[CrossRef](#)]
39. Maniar, P.D.; Piccoli, P.M. Tectonic discrimination in of granitoids. *Geol. Soc. Am. Bull.* **1989**, *01*, 635–643. [[CrossRef](#)]
40. Rollinson, H.R. *Using Geochemical Data: Evaluation, Presentation, Interpretation*; Longman: London, UK, 1993; pp. 1–352.
41. Frost, B.R.; Barnes, C.G.; Collins, W.J.; Arculus, R.J.; Ellis, D.J.; Frost, C.D. A Geochemical Classification for Granitic Rocks. *J. Petrol.* **2001**, *42*, 2033–2048. [[CrossRef](#)]
42. Wilson, M. *Igneous Petrogenesis*; Springer: London, UK, 1989; pp. 295–323.
43. Boynton, W.V. Geochemistry of the rare earth elements: Meteorite studies. In *Rare Earth Element Geochemistry*; Henderson, P., Ed.; Elservier: Amsterdam, The Netherlands, 1984; pp. 63–114.
44. Sun, S.S.; McDonough, W.F. Chemical and isotopic systematics of oceanic basalts: Implications for mantle composition and processes. *Geol. Soc. Spec. Publ.* **1989**, *42*, 313–345. [[CrossRef](#)]
45. Whalen, J.B.; Currie, K.L.; Chappell, B.W. A-type granites: Geochemical characteristics discrimination and petrogeneisis. *Contrib. Mineral. Petrol.* **1987**, *95*, 407–419. [[CrossRef](#)]
46. Wu, F.Y.; Li, X.H.; Yang, J.G.; Zheng, Y.F. Discussions on the petrogenesis of granite. *Acta Petrol. Sin.* **2007**, *23*, 1217–1238.
47. King, P.L.; White, A.J.R.; Chappell, B.W.; Allen, C.M. Characterization and origin of aluminous A-type granites from the Lachlan Fold Belt, Southeastern Australia. *J. Petrol.* **1997**, *38*, 371–391. [[CrossRef](#)]
48. Chen, G.C.; Pei, X.Z.; Li, R.B.; Li, Z.C.; Pei, L.; Liu, C.J.; Chen, Y.X.; Wang, M.; Gao, F.; Li, X.B. Lithospheric extension of the post-collision stage of the Paleo-Tethys oceanic system in the East Kunlun Orogenic Belt: Insights from Late Triassic plutons. *Earth Sci. Front.* **2019**, *26*, 191–208. [[CrossRef](#)]
49. Rudnick, R.L.; Gao, S. Composition of the continental crust. *Treatise Geochem.* **2003**, *3*, 1–64.
50. Chappell, B.W.; Bryant, C.J.; Wyborn, D. Peraluminous I-type granites. *Lithos* **2012**, *153*, 142–153. [[CrossRef](#)]
51. Sisson, T.W.; Ratajeski, K.; Hankins, W.B.; Glazner, A.F. Voluminous granitic magmas from common basaltic sources. *Contrib. Mineral. Petrol.* **2005**, *148*, 635–661. [[CrossRef](#)]
52. Sylvester, P.J. Post-collisional strongly peraluminous granites. *Lithos* **1998**, *45*, 29–44. [[CrossRef](#)]
53. Huang, H.; Niu, Y.L.; Nowell, G.; Zhao, Z.D.; Yu, X.H.; Zhu, D.C.; Mo, X.X.; Ding, S. Geochemical constraints on the petrogenesis of granitoids in the East Kunlun Orogenic belt, northern Tibetan Plateau: Implications for continental crust growth through syn-collisional felsic magmatism. *Chem. Geol.* **2014**, *370*, 1–18. [[CrossRef](#)]
54. Guo, A.L.; Zhang, G.W.; Sun, Y.G.; Cheng, S.Y.; Qiang, J. Sr-Nd-Pb isotopic geochemistry of late -Paleozoic mafic volcanic rocks in the surrounding areas of the Gonghe basin, Qinghai Province and geological implications. *Acta Petrol. Sin.* **2007**, *23*, 747–754.
55. Yu, N.; Jin, W.; Ge, W.C.; Long, X.P. Geochemical study on peraluminous granite from Jinshuikou in East Kunlun. *Glob. Geol.* **2005**, *24*, 123–128.
56. Shao, F.L.; Niu, Y.L.; Liu, Y.; Chen, S.; Kong, J.J.; Duan, M. Petrogenesis of Triassic granitoids in the East Kunlun Orogenic Belt, northern Tibetan Plateau and their tectonic implications. *Lithos* **2017**, *282–283*, 33–44. [[CrossRef](#)]
57. Patiño-Douce, A.E. What do experiments tell us about the relative contributions of crust and mantle to the origin of the granitic magmas? In *Understanding Granites: Integrating New and Classical Techniques*; Castro, A., Fernandez, C., Vigneresse, J.L., Eds.; Geological Society: London, UK, 1999; Volume 168, pp. 55–75.
58. Altherr, R.; Holl, A.; Hegner, E.; Langer, C.; Kreuzer, H. High-potassium, calcalkaline I-type plutonism in the European Variscides: Northern Vosges (France) and northern Schwarzwald (Germany). *Lithos* **2000**, *50*, 51–73. [[CrossRef](#)]
59. Rapp, R.P.; Watson, E.B. Dehydration melting of metabasalt at 8–32 kbar: implications for continental growth and crust–mantle recycling. *J. Petrol.* **1995**, *36*, 891–931. [[CrossRef](#)]
60. Rapp, R.P.; Shimizu, N.; Norman, M.D.; Applegate, G.S. Reaction between slab-derived lelts and peridotite in the mantle wedge: experimental constraints at 3.8Gpa. *Chem. Geol.* **1999**, *160*, 335–356. [[CrossRef](#)]
61. Stevens, G.; Villaros, A.; Moyen, J.F. Selective peritectic garnet entrainment as the origin of geochemical diversity in S-type granites. *Geology* **2007**, *35*, 9–12. [[CrossRef](#)]
62. Castro, A. Tonalite–granodiorite suites as cotectic systems: A review of experimental studies with applications to granitoid petrogenesis. *Earth-Sci. Rev.* **2013**, *124*, 68–95. [[CrossRef](#)]
63. Chen, G.C.; Pei, X.Z.; Li, R.B.; Li, Z.C.; Liu, C.J.; Chen, Y.X.; Xu, T.; Zhang, Y.M. Genesis of magma mixing and mingling of Xiangjiananshan granite batholith in the eastern section of East Kunlun Orogen. *Earth Sci. Front.* **2016**, *23*, 226–240.
64. Defant, M.J.; Drummond, M.S. Derivation of some modern magmas by melting of young subducted lithosphere. *Nature* **1990**, *347*, 662–665. [[CrossRef](#)]
65. Atherton, M.P.; Petford, N. Generation of sodium-rich magmas from newly underplated basaltic crust. *Nature* **1993**, *362*, 144–146. [[CrossRef](#)]

66. Yan, Z.; Bian, Q.G.; Korchagin, O.A.; Pospelov, I.I.; Li, J.L.; Wang, Z.Q. Provenance of Early Triassic Hongshuichuan Formation in the southern margin of the East Kunlun Mountains: Constraints from detrital framework, heavy mineral analysis and geochemistry. *Acta Petrol. Sin.* **2008**, *24*, 1068–1078.
67. Chen, G.C.; Pei, X.Z.; Li, R.B.; Li, Z.C.; Liu, C.J.; Chen, Y.X.; Pei, L.; Ding, S.P. Geological Characteristics and Tectonic Significance of Jurassic Yangqu Formation from Alake Lake in the Eastern Part of East Kunlun Orogenic Belt. *Northwestern Geology* **2017**, *50*, 113–125.
68. Petford, N.; Atherton, M. Na-rich partial Melts form Newly Underplated Basaltic Crust: The Cordillera Blanca Batholith, Peru. *J. Petrol.* **1996**, *37*, 1491–1521. [CrossRef]
69. Castillo, P.R. An overview of adakites petrogenesis. *China Sci. Bull.* **2006**, *51*, 257–268. [CrossRef]
70. Zhang, L.Y.; Li, S.S.; Zhao, Q.Y. A review of research on adakites. *Int. Geol. Rev.* **2021**, *63*, 47–64. [CrossRef]
71. Castillo, P.R. Adakite petrogenesis. *Lithos* **2012**, *134–135*, 304–316. [CrossRef]
72. Watson, E.B.; Harrison, T.M. Zircon saturation revisited: Temperature and composition effects in a variety of crustal magma types. *Earth Planet. Sci. Lett.* **1983**, *64*, 295–304. [CrossRef]
73. Lieu, W.H.; Stern, R.J. The robustness of Sr/Y and La/Yb as proxies for crust thickness in modern arcs. *Geosphere* **2019**, *15*, 621–641. [CrossRef]
74. Chen, B.; Jahn, B.M.; Arakawa, Y.; Zhai, M.G. Petrogenesis of Mesozoic intrusive complexes from the southern Taihang Orogen, North China Craton: Elemental and Sr–Nd–Pb isotopic constraints. *Contrib. Mineral. Petrol.* **2004**, *148*, 489–501. [CrossRef]
75. Wang, Q.; Xu, J.F.; Jian, P.; Bao, Z.W.; Zhao, Z.H.; Li, C.F.; Xiong, X.L.; Ma, J.L. Petrogenesis of adakitic porphyries in an extensional tectonic setting, Dexing, South China: Implications for the genesis of porphyry copper mineralization. *J. Petrol.* **2006**, *47*, 119–144. [CrossRef]
76. Wang, X.L. Some new research progresses and main scientific problems of granitic rocks. *Acta Petrol. Sin.* **2017**, *35*, 1445–1458.
77. Gao, S.; Rudnick, R.L.; Yuan, H.L.; Liu, X.M.; Liu, Y.S.; Xu, W.L.; Ling, W.L.; Ayers, J.; Wang, X.C.; Wang, Q.H. Recycling lower continental crust in the North China Craton. *Nature* **2004**, *432*, 892–897. [CrossRef] [PubMed]
78. Patiño-Douce, A.E.; Johnston, A.D. Phase equilibria and melt productivity in the pelitic system: Implications for the origin of peraluminous granitoids and aluminous granulites. *Contrib. Mineral. Petrol.* **1991**, *107*, 202–218. [CrossRef]
79. Patiño-Douce, A.E.; Harris, N. Experimental constraints on Himalayan anatexis. *J. Petrol.* **1998**, *39*, 689–710. [CrossRef]
80. Rushmer, T. Granulites as residues of partial melting: Experimental constraints. *Terra Abstr.* **1989**, *1*, 302.
81. Collins, W.J.; Huang, H.Q.; Jiang, X.Y. Water-fluxed crustal melting produces Cordilleran batholiths. *Geology* **2016**, *44*, 143–146. [CrossRef]
82. Moyen, J.F.; Stevens, G.; Kisters, A. Record of mid–Archaean subduction from metamorphism in the Barberton terrain, South Africa. *Nature* **2006**, *442*, 559–562. [CrossRef]
83. Li, S.; Chung, S.L.; Wang, T.; Wilde, S.A.; Chu, M.F.; Pang, C.J.; Guo, Q.Q. Water-fluxed crustal melting and petrogenesis of largescale Early Cretaceous intracontinental granitoids in the southern Great Xing'an Range, North China. *Geol. Soc. Am. Bull.* **2018**, *130*, 580–597. [CrossRef]
84. Storre, B.; Karotke, E. Experimental data on melting reactions of muscovite+ quartz in the system $K_2O-Al_2O_3-SiO_2-H_2O$ to 20 kbarwater pressure. *Contrib. Mineral. Petrol.* **1972**, *36*, 343–345. [CrossRef]
85. Long, L.; Sial, A.; Nekvasil, H.; Borba, G. Origin of granite at Cabo de Santo Agostinho, northeast Brazil. *Contrib. Mineral. Petrol.* **1986**, *92*, 341–350. [CrossRef]
86. Anderson, J.L.; Bender, E.E. Nature and origin of Proterozoic A-type granitic magmatism in the southwestern United States of America. *Lithos* **1989**, *23*, 19–52. [CrossRef]
87. Chen, J.; Wang, B.Z.; Li, B.; Zhang, Z.Q.; Qiao, B.X.; Jin, T.T. Zircon U–Pb ages, geochemistry and Sr–Nd–Pb isotopic compositions of Middle Triassic granodiorites from the Kaimuqi area, East Kunlun, Northwest China: Implications for slab breakoff. *Int. Geol. Rev.* **2015**, *57*, 257–270. [CrossRef]
88. Chen, G.C.; Pei, X.Z.; Li, R.B.; Li, Z.C.; Liu, C.J.; Chen, Y.X.; Pei, L.; Li, X.B.; Wang, M. Magma Mixing and Mingling for Xiangjiananshan Granitic batholith at eastern area of the East Kunlun Orogenic Belt. *Acta Geol. Sin.–Engl.* **2017**, *91*, 63. [CrossRef]
89. Chen, G.C.; Pei, X.Z.; Li, R.B.; Li, Z.C.; Liu, C.J.; Chen, Y.X.; Pei, L.; Wang, M.; Li, X.B.; Zhang, Y. Age and Petrogenesis of Jialuhe Basic–Intermediate Pluton in Xiangjia'nanshan Granite Batholith in the Eastern Part of East Kunlun Orogenic Belt and its Geological Significance. *Geotecton. Metallog.* **2017**, *41*, 1097–1115.
90. Chen, J.J.; Wei, J.H.; Fu, L.N.; Li, H.; Zhou, H.Z.; Zhao, X.; Zhan, X.F.; Tan, J. Multiple sources of the Early Mesozoic Gouli batholith, Eastern Kunlun Orogenic Belt, northern Tibetan Plateau: Linking continental crustal growth with oceanic subduction. *Lithos* **2017**, *292*, 161–178. [CrossRef]
91. Xin, W.; Sun, F.Y.; Zhang, Y.T.; Fan, X.Z.; Wang, Y.C.; Li, L. Mafic–intermediate igneous rocks in the East Kunlun Orogenic Belt, northwestern China: Petrogenesis and implications for regional geodynamic evolution during the Triassic. *Lithos* **2019**, *346–347*, 105159. [CrossRef]
92. Pearce, J.A.; Harris, B.W.; Tindie, A.G. Trace element discrimination diagrams for the tectonic interpretations of granitic rocks. *J. Petrol.* **1984**, *25*, 956–983. [CrossRef]
93. Batchelor, R.A.; Bowden, P. Petrogenetic interpretation of granitoid rock series using multicationic parameters. *Chem. Geol.* **1985**, *48*, 43–45. [CrossRef]

94. Whalen, J.B.; Hildebrand, R.S. Trace element discrimination of arc, slab failure, and A-type granitic rocks. *Lithos* **2019**, *348–349*, 105179. [[CrossRef](#)]
95. Zhang, J.Y.; Ma, C.Q.; Xiong, F.H.; Liu, B. Petrogenesis and tectonic significance of the Late Permian–Midele Triassic calc–alkaline granites in the Balong region, eastern Kunlun Orogen, China. *Geol. Mag.* **2012**, *149*, 892–908. [[CrossRef](#)]
96. Xiong, F.H.; Ma, C.Q.; Zhang, J.Y.; Liu, B.; Jiang, H.A. Reworking of old continental lithosphere: An important crustal evolution mechanism in orogenic belts, as evidenced by Triassic I-type granitoids in the East Kunlun orogen, Northern Tibetan Plateau. *J. Geol. Soc. Lond.* **2014**, *171*, 847–863. [[CrossRef](#)]
97. Xiong, F.H.; Ma, C.Q.; Chen, B.; Ducea, M.N.; Hou, M.C.; Ni, S.J. Intermediate–mafic dikes in the East Kunlun Orogen, Northern Tibetan Plateau: A window into paleo-arc magma feeding system. *Lithos* **2019**, *340–341*, 152–165. [[CrossRef](#)]
98. Liegeois, G.P. Preface—some words on the post-collisional magmatism. *Lithos* **1998**, *45*, 1–14.
99. Yu, M.; Feng, C.Y.; Zhao, Y.M.; Li, D.X. Genesis of post-collisional calc–alkaline and alkaline granitoids in Qiman Tagh, East Kunlun, China. *Lithos* **2015**, *239*, 45–59. [[CrossRef](#)]
100. Ding, S.; Huang, H.; Niu, Y.L.; Zhao, Z.D.; Yu, X.H.; Mo, X.X. Geochemistry, geochronology and petrogenesis of East Kunlun high Nb–Ta rhyolites. *Acta Petrol. Sin.* **2011**, *27*, 3603–3614.
101. Luo, M.F.; Mo, X.X.; Yu, X.H.; Li, X.W.; Huang, X.F.; Yu, J.C. Zircon LA–ICP–MS U–Pb age dating, petrogenesis and tectonic implications of the Late Triassic granites from Xiangride area, East Kunlun. *Acta Petrol. Sin.* **2014**, *30*, 3229–3241.
102. Xia, R.; Wang, C.M.; Deng, J.; Carranza, E.J.M.; Li, W.L.; Qing, M. Crustal thickening prior to 220Ma in the East Kunlun Orogenic Belt: Insights form the Late Triassic granitoids in the Xiao–Nuomuhong pluton. *J. Asian Earth Sci.* **2014**, *93*, 193–210. [[CrossRef](#)]